Energy Conversion and Management 353 (2026) 121206

Contents lists available at ScienceDirect

Energy Conversion and Management

journal homepage: www.elsevier.com/locate/enconman

Research Paper

Conventional and PCM-based heat recovery configurations for hybrid electric heavy-duty vehicles fuelled with fossil or alternative fuels

Pietropaolo Morrone [a], Paolo Cutuli [a], Talha Mujahid [b], Angelo Algieri [a], Luigi Falbo [a], Teresa Donateo [b,*]

[a] Department of Mechanical, Energy and Management Engineering (DIMEG), University of Calabria, Via P. Bucci, Rende (CS) 87036, Italy
[b] Department of Engineering for Innovation, University of Salento, via Monteroni, Lecce 73100, Italy

ARTICLE INFO

Keywords:
Waste heat recovery (WHR)
Organic Rankine Cycle (ORC)
Phase Change Material (PCM)
Heavy-duty vehicle electrification
Dynamic driving conditions

ABSTRACT

Hard-to-electrify transportation systems, such as heavy-duty vehicles, still rely on thermal engines because of their high energy demands, which current battery technologies cannot yet meet. In this context, waste heat recovery (WHR), combined with electrification and the adoption of carbon–neutral fuels, represents a key strategy to enhance efficiency and reduce emissions.

The IRIDESCENT project ("biodIesel hybRID Electric buS with waste heat reCovEry aNd sTorage") aims to exploit synergies among hybridization, WHR, and biodiesel use to achieve carbon neutrality and mitigate cold-start emissions in heavy-duty vehicles. Within this framework, the present study proposes a WHR system that integrates Organic Rankine Cycles (ORCs) with Phase Change Materials (PCMs) to buffer thermal fluctuations, thereby enabling extended ORC operation under variable load conditions.

The design and off-design analyses of the proposed advanced WHR system are carried out using real-world data. A comprehensive dataset of 28 real driving trips acquired from a heavy-duty vehicle is analyzed to capture the variability of exhaust gas temperature and flow rate under dynamic conditions. A quasi-static engine model combined with a frequency-domain analysis, based on a modified rectangle criterion, is employed for the WHR design.

For the ORC, a sensitivity analysis is performed considering different configurations and working fluids. At the same time, a novel optimization method is developed to determine the optimal melting temperature of the PCM, identifying potassium nitrate (KNO_3) as the most suitable material. Results show that PCM integration enhances ORC efficiency by up to 18.5% and WHR efficiency by up to 11.3%, while maintaining a utilization factor above 96%, thus confirming its effectiveness under dynamic driving conditions. The regenerative ORC configuration with R245fa and PCM integration achieved the best performance, demonstrating the feasibility of a compact, lightweight WHR system for sustainable heavy-duty transportation.

1. Introduction

Heavy-duty vehicles (HDVs), such as trucks and buses, account for approximately 25% of CO_2 emissions from road transport in the European Union, despite being a small share of the road vehicle fleet. To address this, the European Commission has recently established two sets of CO_2 emission limits, covering both hot and cold conditions. Under these regulations, new large trucks must reduce their CO_2 emissions by 30% compared to current levels, with an interim target of 15% by 2025. Identifying effective strategies to mitigate environmental impacts is urgent, especially since HDVs entering the market before 2035 are expected to remain in operation for many years.

Environmental regulators have steadily tightened HDV emission standards over the past decade. The Euro VI standard (in effect since 2013) mandated advanced aftertreatment systems, dramatically reducing allowable NO_x and PM. However, real-world tests revealed challenges in controlling emissions during cold-start and low-load operations, when exhaust aftertreatment is least effective [1]. In response, upcoming Euro VII regulations are being formulated with even stricter limits, including dedicated provisions for cold-start emissions and urban driving conditions [2].

Meeting these goals is challenging with current diesel engine technology. Even modern heavy-duty diesel engines achieve a brake thermal

* Corresponding author.
E-mail address: teresa.donateo@unisalento.it (T. Donateo).

https://doi.org/10.1016/j.enconman.2026.121206
Received 4 December 2025; Received in revised form 23 January 2026; Accepted 6 February 2026
Available online 16 February 2026
0196-8904/© 2026 The Author(s). Published by Elsevier Ltd. This is an open access article under the CC BY license (http://creativecommons.org/licenses/by/4.0/).

Nomenclature

Symbols

A	Heat exchanger area m^2
c_p	Specific heat capacity $kJ/kg\ K$
Δt	Time interval s
E	Energy kJ
η	Efficiency –
k	Thermal conductivity
λ	PCM latent heat kJ/kg
m	Mass kg
$\dot{m}$	Mass flow rate kg/s
n	Engine speed rpm
Nu	Nusselt Number –
P	Power kW
ρ	Density Kg/m^3
Q	Thermal power kW
T	Temperature $^\circ C$
U	Heat Exchange Coefficient W/m^2K
V	Velocity m/s

Subscripts/Superscripts

act	Actual quantity admitted to the system (after regulation)
aux	Auxiliary
e	expander
exh	Exhaust
el	Electric
em	Electro-mechanical
gb	Global
filt	Filtered
F	Fuel
in	Inlet
is	Isentropic
log	Logarithmical
max	Maximum
melt	Melting
min	Minimum
of	Organic Fluid
out	Outlet
nom	Nominal load
part	Partial load
pc	Pseudo-Critical
p	Pump
Pr	Prandtl number
Re	Reynolds number
SIM	SIMPLE
th	thermal
t	Traction
tot	Total

Acronyms

HDV	Heavy Duty Vehicle
HEX	Heat Exchanger
HRVG	Heat Recovery Vapor Generator
ICE	Internal Combustion Engine
IHE	Internal Heat Exchanger
OBD	On-Board Diagnostics
ORC	Organic Rankine Cycle
PCM	Phase Change Material
PHE	Plate Heat Exchanger
PM	Particulate Matter
STHE	Shell-and-tube
TES	Thermal Energy Storage
TORC	Transcritical Organic Rankine Cycle
WHR	Waste Heat Recovery

efficiency of at best 43–46% [3], meaning that well over half of the fuel's energy is lost as waste heat. A substantial portion of the fuel energy (typically 20–30% or more) is lost from the engine in the form of high-temperature exhaust gases [4], with additional energy being lost to the engine coolant and other thermal losses. These inefficiencies not only waste fuel (increasing CO_2 emissions) but also represent an opportunity. If some of this waste heat can be recovered and converted to useful work, the overall vehicle efficiency can be improved. Indeed, effective recovery of HDV waste heat is identified as a key strategy for meeting increasingly stringent fuel economy and CO_2 standards [5].

Heavy-duty vehicles belong to the so-called "hard to electrify" transportation systems, where thermal engines are not expected to be banished in the near future, and achieving carbon neutrality will require adopting biofuels and e-fuels. Therefore, waste-heat recovery remains relevant to HDVs.

WHR with an Organic Rankine Cycle is a viable solution for converting residual thermal energy into mechanical or electrical power [6], either back to the drivetrain or to vehicle auxiliaries. ORC can achieve net efficiencies of up to 8% [7]. However, implementing ORC systems in transportation poses challenges due to space constraints and system complexity.

The ORC is a mature technology capable of transforming low- to medium-temperature heat sources into usable work or electricity. Yang et al. [8] analyzed the performance of a subcritical ORC system in a fully loaded heavy-duty truck and reported fuel economy improvements ranging from 4.48% to 7.52% under various driving conditions. Similarly, Zhao et al. [9] conducted simulations using real-world driving cycles from Europe, the U.S., and China, finding reductions in fuel consumption of 2.5%, 3.1%, and 3.4%, respectively, depending on the region-specific cycle characteristics.

The recovered energy can be converted either into mechanical power, transmitted to the crankshaft, or into electrical power via a generator. Possible uses of the electrical output include powering auxiliary loads (e.g., a radiator fan or an air conditioning compressor) or charging the battery in hybrid electric configurations (Mahmoudzadeh et al. [10]). Thantla et al. [11] explored a dual-loop ORC configuration and found that it not only enhanced thermal efficiency but also improved adaptability to dynamic engine load conditions, a critical feature for real-world operations. In fact, in the application of HDVs, the WHR system design must accommodate several constraints, including limited installation space, fluctuating thermal loads from exhaust gases, and the need for robust, autonomous operation. Conventional ORC adds extra components, such as heat exchangers, a working fluid circuit, an expander, a condenser, and a pump, which increases the vehicle's weight and complexity. This added mass can partly offset the efficiency gains by increasing the vehicle's fuel consumption; for example, a review found that ORC components, which increase system weight by about 10%, can measurably deteriorate overall fuel economy [12]. Moreover, the thermal operating profile of a vehicle engine is highly dynamic, including engine load and exhaust heat flow that can fluctuate rapidly with driving conditions (such as accelerations, decelerations, and idle periods). Fast changes in exhaust temperature or flow can lead to inefficient operation or even necessitate bypassing the ORC to protect it [13]. During sudden drops in engine load, a traditional ORC may not ingest sufficient heat to sustain vaporization, leading to a decrease in expander power or premature condensation of the working fluid. At very low loads or during engine warm-up, exhaust gas temperatures can be below the ORC's minimum operating range, rendering the WHR system

inactive exactly when the engine is least efficient.

The sizing of the WHR can be performed with several methods. In heavy-duty applications, sizing is usually performed by considering highway driving conditions, where the engine is assumed to operate at a constant speed and load [14]. In the investigation by Villani et al. [15], the most frequent working condition of the engine (torque and speed) occurred during the HHDDY driving cycle. However, this could not correspond to the most frequent thermal energy availability. Lion et al. [16] pointed out the importance of studying real-life operating profiles for the design and optimization of the WHR system and to take into account not only the point at which the engine spends most of its time but also the suitability of such optimum points in terms of exhaust mass flows and temperature levels. For this reason, this investigation proposes a modified version of the classical "maximum rectangle" method [17], originally developed for the sizing of stationary power systems such as Combined Cooling, Heating, and Power systems [18], as well as stationary engines or ORCs, with the aim of stationary energy production [19]. Our version of this method accounts for the highly variable load profiles of automotive engines by considering energy recovery during partial-load operation based on the frequency–duration distribution of exhaust thermal power. In addition, integrating PCMs allows buffering thermal fluctuations and extending the duration of ORC operation at nominal conditions.

Instead of using traditional chassis dynamometer testing [14] or model-based analyses of standard driving cycles [15], this investigation considers highly variable real-driving data acquired with a Portable Emissions Measurement System (PEMS), combined with data from the On-Board Diagnostics (OBD) and GPS systems [20].

To handle the significant variability in engine load and speed under real-world conditions, PCMs are proposed. PCMs offer substantially higher thermal storage capacities compared to conventional sensible heat storage systems [21]. Heat exchangers incorporating PCMs can buffer temperature fluctuations in the exhaust stream of internal combustion engines (ICEs), improving WHR system efficiency by storing thermal energy from 6 to 15 h [22], effectively minimizing cold-start events with adequate insulation.

In HEVs, unlike conventional vehicles that typically experience a single cold start per trip, the ICE operates intermittently, making it more prone to frequent cold starts. Insufficient heating in these phases reduces engine efficiency [23] and compromises the performance of aftertreatment systems. By integrating PCM-based storage, it is possible to retain engine warmth after shutdown by leveraging residual heat from the previous operation.

In summary, the present investigation proposes an innovative and comprehensive sizing procedure for a WHR system comprising a PCM heat exchanger and an ORC unit, designed for integration into the hybrid electric powertrain. The low-temperature recovery from the coolant circuit, which is technically feasible but less energy-dense, is here neglected.

The innovative contribution of the investigation is here summarized:

1. Transcritical ORC arrangements are analyzed to explore the maximum recovery potential of WHR systems, a topic rarely addressed in automotive applications [24].
2. A novel optimization study is introduced to find the optimal melting temperature of PCM.
3. A modified version of the "maximum rectangle" method, initially developed for stationary energy systems, is adopted to handle partial-load operation and PCM-based thermal buffering under highly variable automotive exhaust conditions.
4. While the thermodynamic model for the ORC system is based on our previously validated work [17], the evaporator model, which establishes the thermal coupling between the engine and the ORC, has been developed specifically for this study.
5. The dynamicity of the mass flow rate and temperature of exhaust gases is obtained from analysis of experimental data acquired under real-world operating conditions, integrated with a quasi-static model of a heavy-duty vehicle.
6. Rather than tracking the instantaneous evolution of thermal power, the analysis focuses on the statistical distribution of exhaust energy availability over time. This allows the identification of the most frequent operating conditions and the corresponding thermal power levels.
7. The design of the WHR unit is based on a frequency analysis of a dataset comprising 28 driving cycles.
8. A sensitivity study on the configurations and fluids for the ORC and the Heat Exchanger (HEX) is performed.
9. It estimates the mass and volume of the WHR, which directly affects the vehicle's payload capacity and overall efficiency.

Note that, even though the procedure and results are based on experimental data from a fossil-fueled diesel engine, they can be extended to biodiesel and e-fuels.

The rest of the paper is organized as follows. Section 2 presents the proposed integrated WHR system, whose design methodology is illustrated in Section 3. Section 4 describes the frequency analysis of engine exhaust gases based on an open-access database to identify the engine operating condition that maximizes waste heat recovery. Section 5 discusses the results and compares the proposed configuration in terms of global performance indexes. To improve the paper's readability, the modeling approaches for the engine and the WHR are reported in the Appedix.

2. Proposed power system

The IRIDESCENT project ("biodIesel hybRID Electric buS with waste heat reCovEry aNd sTorage"), supported by the European Union – NextGenerationEU via the Italian Ministry of University and Research (MUR), has the goal of minimizing the environmental impact of heavy-duty vehicles, specifically during real-world driving conditions, including cold start operations. This goal is to be achieved by leveraging synergy among WHR using the ORC, hybridization, biodiesel use, and Thermal Energy Storage (TES) systems. This investigation focuses on the WHR system, which receives energy from the exhaust gases of a compression-ignition engine in the Isuzu FTR850 via a Heat Exchanger (HEX). Both sensible-heat and PCM-based HEXs are considered. The other sources of heat from the engine (exhaust gas recirculation, coolant, lube oil, and charge air cooling) are not considered in this investigation, since it is not practical to recover energy from multiple heat sources in vehicle applications [16].

The electricity generated by the ORC is summed to the battery current to feed the electric machine. The electric machine's mechanical power is combined with the engine's mechanical output to power the vehicle, as required by the parallel hybridization scheme. The auxiliaries are meant to be powered by electric drives. Losses of energy in all components of the power system (engine, electric machine, HEX, ORC, and battery) are considered.

The distribution of energy flows in the power system is illustrated in the qualitative Sankey diagram of Fig. 1, which corresponds to a parallel hybrid electric architecture proposed in a previous investigation. Other thermal losses of the engine, such as power dissipated through coolant, lubricant oil, mechanical friction, pumping work, and radiation, are denoted as "cooling + rad". The presence of aftertreatment devices is assumed not to contribute to the thermal flow, i.e., the temperature change across the aftertreatment system is assumed to be negligible, as suggested by Villani et al. [15].

A preliminary analysis performed by Donateo et al. [25] showed that the adoption of the proposed WHR can improve fuel consumption (−3.5%) or reduce the size of the battery (−16%), provided that the ORC can generate an average power of 2 kW, as required by the auxiliaries of the vehicle.

Fig. 2 illustrates the conventional WHR system layouts, which serve

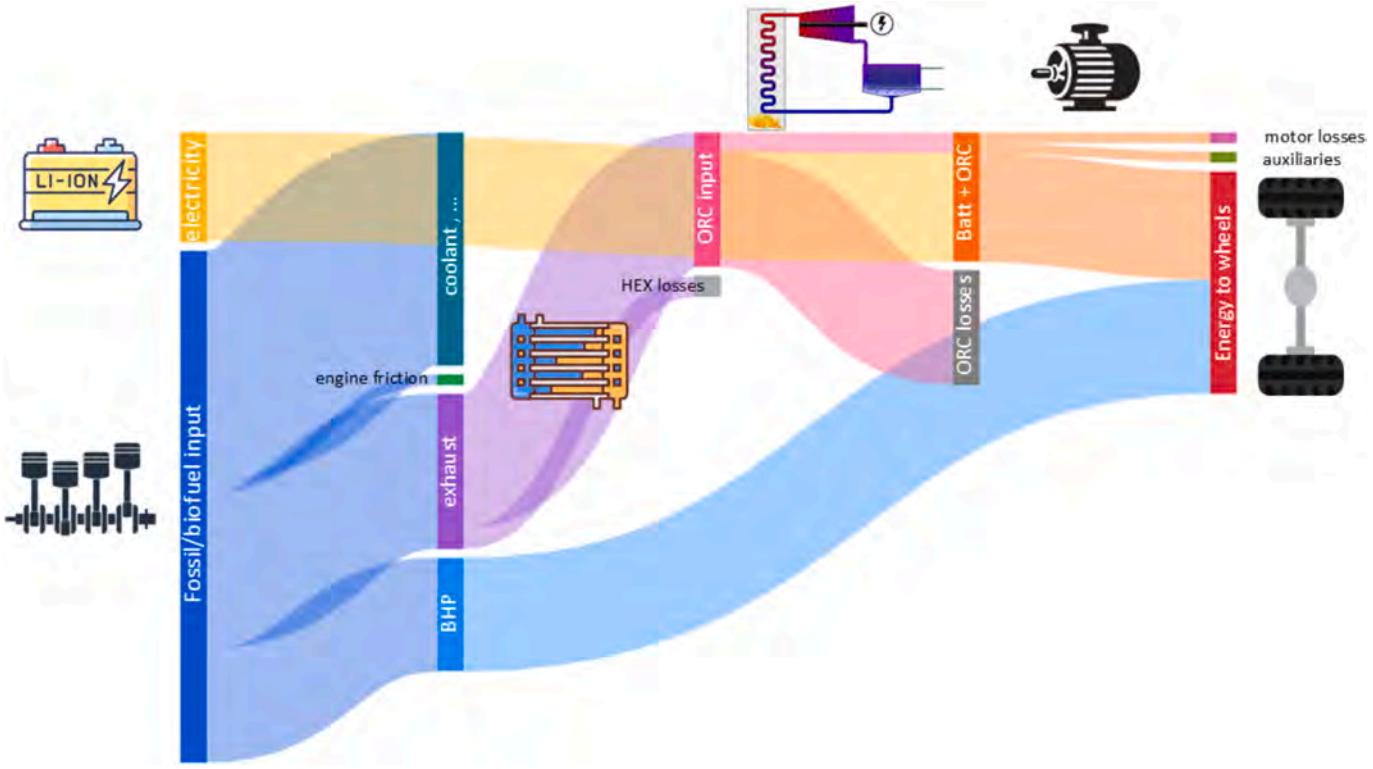

Fig. 1. Qualitative Sankey diagram of the proposed power system.

as the baseline for comparison with the PCM-based solution. The ORC core includes the evaporator, the expander, the condenser, and an electric pump decoupled from the expander to enable partial-load operation. The working fluid is pumped to high pressure, preheated, and vaporized in the heat exchanger using exhaust gas energy. The vapor then expands in the turbine, producing mechanical power, and is finally condensed before being recirculated. The regenerative configuration integrates an Internal Heat Exchanger (IHE) to improve cycle efficiency by preheating the working fluid before entering the evaporator. The simple (a) and regenerative (b) ORC configurations operate under transcritical conditions. The transcritical layout was selected for detailed analysis due to its higher potential for energy recovery at medium-to-high exhaust temperatures. This choice aligns with prior engine waste-heat recovery works on supercritical cycles [26].

In the application to a vehicle, the WHR encounters a range of conditions, requiring a flexible control strategy to ensure safe and efficient operation. Fig. 2 also illustrates how the WHR system adapts to variable exhaust conditions. A dedicated valve-based control strategy is implemented to regulate the exhaust gas flow entering the evaporator, i.e., the HRVG (Heat Recovery Vapor Generator), and ensure efficient and safe operation. The valve bypasses the WHR system whenever thermodynamic conditions fall outside the acceptable range for the heat exchanger, i.e., when the exhaust temperature and/or mass flow rate are excessive or insufficient. The control logic also aims to maintain the nominal thermal input for as long as possible. When exhaust thermal power exceeds the nominal value, the valve throttles the flow to preserve the design input as long as possible and prevent organic fluid chemical degradation. Conversely, if the available thermal power drops below the nominal threshold, the ORC operates at partial load or is temporarily shut down. Although this approach slightly reduces instantaneous efficiency, it significantly extends the ORC system's cumulative operating time. As discussed in the following paragraphs, PCM integration further enhances this strategy by enabling longer operation at nominal conditions through thermal buffering.

A critical aspect of WHR integration is heat dissipation at the condenser, which strongly influences system performance and packaging. For this reason, an air-cooled condenser was selected as a practical trade-off between thermal performance, system simplicity, and the need to minimize WHR weight. In this quasi-static framework, the condenser is not modeled explicitly. Instead, the ORC is evaluated at fixed condensing-temperature setpoints (30 °C, 40 °C, 50 °C), consistent with off-design studies that hold the condensing temperature constant [27]. Full ORC model details are in the Appendix.

3. Design methodology

The sizing of the WHR performed in this investigation is based on the maximum rectangle method [19]. It relies on a quasi-static frequency analysis of the thermal power available under real-world driving conditions.

Fig. 3 illustrates the methodological principle of the "maximum rectangle" criterion. This criterion determines the nominal thermal power input for the WHR system that maximizes the total recoverable energy, assuming the flow control strategy described earlier. The method is based on the following steps:

1) For each exhaust thermal power level, the corresponding cumulative duration is calculated, and the grey area of Fig. 3 is obtained.
2) The value of $\dot{Q}_{exh}$ which maximizes the area of the rectangle $\dot{Q}_{exh} \bullet d$ is found (red area of Fig. 3). This value of $\dot{Q}_{exh}$ corresponds to the nominal power level for the WHR system, while d is time at which the system can operate at nominal load. The nominal load will be used to evaluate conversion efficiency and net power output through the ORC and heat exchanger models.
3) At partial-load conditions, the WHR can absorb lower thermal inputs up to the minimum ORC load, Q_{min}. This operating condition corresponds to the blue trapezium of Fig. 3.
4) The sum of the two contributions gives the total recoverable energy: the energy corresponding to the nominal power level (red rectangle),

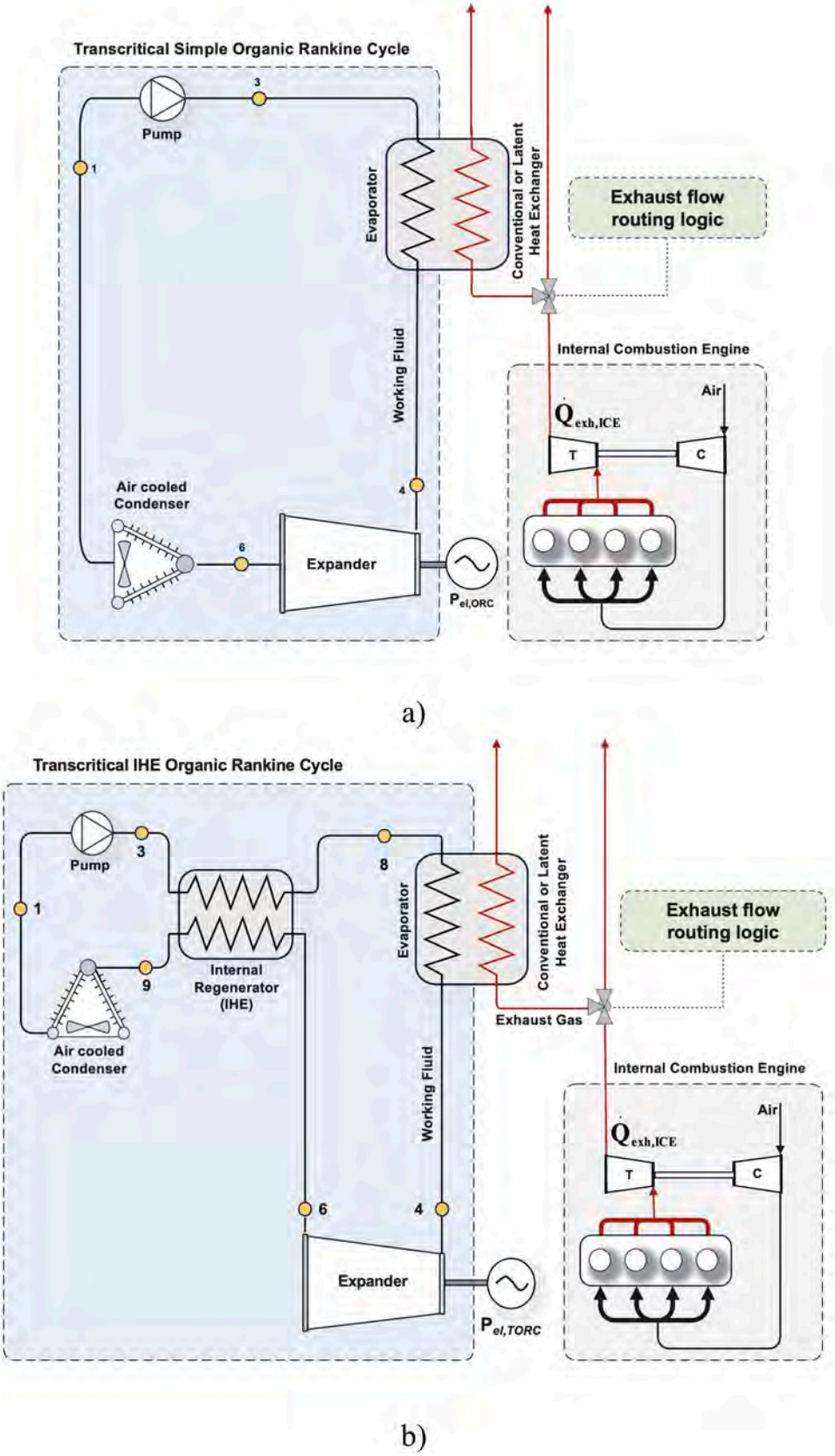

Fig. 2. WHR plant scheme with conventional or latent heat exchangers: (a) Simple configuration (b) Internal regenerative configuration (IHE); exhaust side bypass valve bypasses the WHR outside admissible temperature/flow ranges.

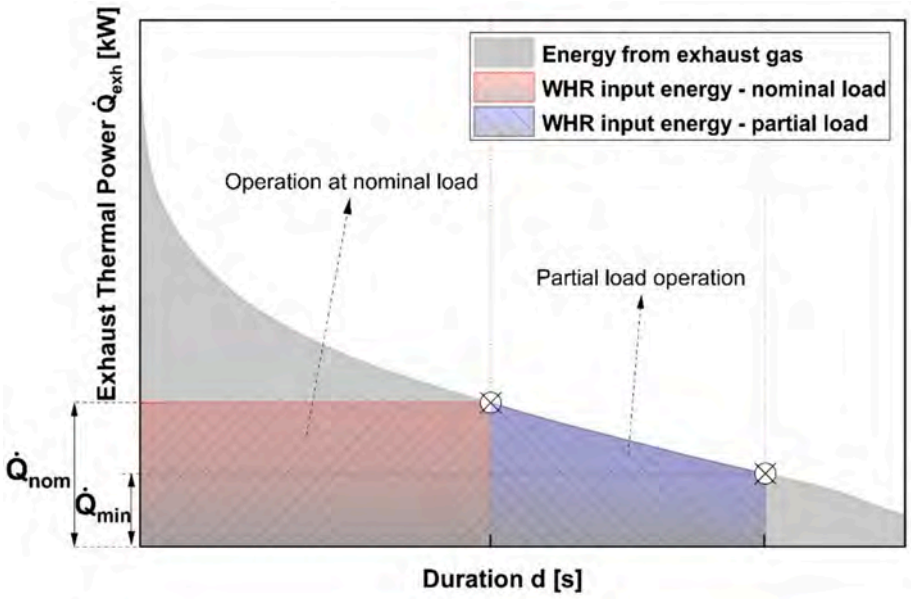

Fig. 3. Frequency-duration diagram and illustration of the maximum rectangle method.

and the additional energy recoverable at partial load (blue trapezium), where the ORC operates below its nominal input.

Under nominal operating conditions, the nominal admitted thermal power at the HRVG inlet under bypass control is the following

$$\dot{Q}_{th,nom}^{exh} = \dot{m}_{nom} c_p^{exh} (T_{exh,nom} - T_{ext,out}) \quad (1)$$

where $T_{ext,out}$ is the design temperature at the exhaust exit (see Appendix).

The electrical energy produced by the ORC at nominal load is calculated as:

$$E_{El,nom,LOAD}^{ORC} = \dot{Q}_{th,nom}^{exh} \Delta t_{nom}{}^{*} \eta_{ORC,nom} \quad (2)$$

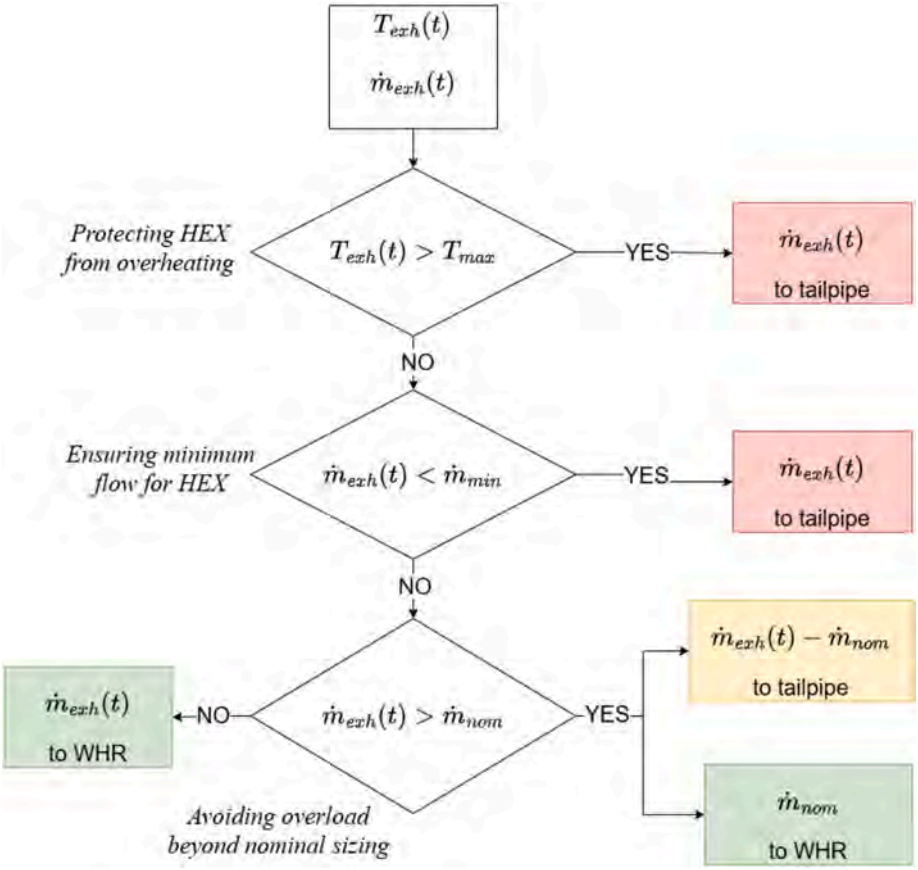

Fig. 4. Exhaust flow routing logic for robust ORC operation.

where Δt_{nom} is the duration corresponding to the nominal power input, $\eta_{ORC,nom}$ is the ORC nominal efficiency, which depends on the system configuration, the selected working fluid, and the condensation temperature. The electrical energy recovered under partial load conditions is given by:

$$E_{el,part}^{ORC} = \int_0^{\Delta t_{nom}} \dot{Q}_{th,act}^{exh}(t)\,\eta_{ORC}(t)dt \tag{3}$$

where $\eta_{ORC}(t)$ is the time-dependent efficiency derived from the ORC performance curves, as described in the following section and $\dot{Q}_{th,act}^{ext}(t)$ denotes the thermal power admitted to the HRVG after bypass valve–action depicted in Fig. 4.

The total electrical energy recovered by the WHR system is therefore the sum of the two contributions:

$$E_{el,tot}^{ORC} = E_{el,nom}^{ORC} + E_{el,part}^{ORC} \tag{4}$$

Finally, the overall ORC and global WHR efficiencies are as follows:

$$\eta_{ORC} = \frac{E_{el}^{ORC}}{E_{in}^{ORC}} \tag{5}$$

$$\eta_{WHR} = \frac{E_{el}^{ORC}}{E_{exh}^{filt}} \tag{6}$$

where E_{in}^{ORC} represents the thermal energy delivered to the ORC cycle through the HRVG over the analysis window, whereas E_{exh}^{filt} denotes the exhaust-side energy that is both available and admissible for recovery after applying the temperature and mass-flow compatibility filters defined in Section 3.

To ensure the safe and efficient operation of the ORC system, i.e., to ensure proper heat exchange and avoid degradation of the organic working fluid, the exhaust gas temperature must be limited. As suggested in the literature [28], the maximum temperature for the organic working fluid can be set to 250 °C, representing a trade-off between thermodynamic performance and fluid stability. However, during partial load operation, the inlet conditions to the expander can vary significantly, with the turbine-inlet temperature decreasing as load is reduced. Accordingly, the maximum exhaust gas temperature entering the heat exchanger, $T_{max,}$ is limited to 380 °C. This choice is also consistent with established practice: in both general ORC applications [29] and engine–coupled WHR [30], the maximum hot–source temperature is 400 °C. Although the internal combustion engine may produce higher exhaust temperatures at full load, a strict cut-off is imposed to preserve the chemical integrity of the organic fluid. On the exhaust side, a minimum temperature of around 90 °C must be maintained to ensure proper operation of the after-treatment system and to avoid condensation-related corrosion. Additionally, an approach temperature difference of approximately 50 °C is required at the heat exchanger to ensure effective thermal transfer between the exhaust gases and the working fluid. Outside this compatibility band, the valve-based bypass limits the admitted temperature and flow. The logic used to avoid overheating, preventing overload beyond nominal sizing is depicted in Fig. 4. The controller uses exhaust admissibility checks on two variables, i.e., exhaust temperature (T_{exh}) and mass flow rate ($\dot{m}_{exh}$). If the exhaust temperature is above the allowed maximum (T_{max}) or the mass flow rate is below the minimum ($\dot{m}_{min}$), the entire stream is bypassed to the tailpipe, and the ORC is temporarily stopped. If the exhaust mass flow rate is higher than the allowed maximum, the valve admits only the nominal flow to the HRVG and routes the excess ($\dot{m}_{exh}$-$\dot{m}_{nom}$) directly to the tailpipe. When conditions are within the admissible range, the valve modulates the admitted flow to keep the thermal input at its nominal value whenever possible, i.e., if the source can provide less than nominal but still above the minimum, the ORC operates at part load. When a PCM unit is present, any surplus thermal energy during high-power phases is stored and later released to extend operation at nominal conditions.

3.1. Phase change materials

In addition to the conventional heat exchanger, this study introduces an innovative configuration based on a PCM, which acts as an intermediate thermal buffer. This configuration employs a dual-channel heat exchanger embedded in a PCM matrix, i.e., a structured system of thermally coupled ducts, designed to act as an intermediate medium between the exhaust gases and the organic working fluid.

The PCM operates most effectively during its melting phase, maintaining a nearly constant temperature. This thermal plateau enables stable heat exchange and decouples exhaust gas fluctuations from ORC operation. Consequently, the selection of the PCM (particularly its melting temperature) is a critical design parameter.

Fig. 5 complements the methodological description by illustrating the architecture of the innovative PCM-based heat exchanger. The left part of the figure shows the layout: one duct network carries the exhaust gases (red arrows), transferring heat to the PCM; the other conveys the organic working fluid (blue arrows), which absorbs the stored energy before entering the ORC. The correct figure presents the temperature profiles along both flow paths, highlighting the PCM's plateau (green line). Note that the PCM-based HRVG corresponds to the latent heat exchanger option in Fig. 2 since the PCM acts as an intermediate thermal buffer between the exhaust stream and the organic working fluid. The exhaust gases enter at a high temperature (T_{EXH}^{in}) and cool down as they transfer heat to the PCM, exiting at T_{EXH}^{out} Simultaneously, the organic fluid enters at a lower temperature (T_{ORC}^{in}) and is heated by the PCM material up to its evaporation temperature (T_{ORC}^{eva}). The green horizontal line represents the PCM melting temperature (T_{PCM}^{melt}), highlighting the phase change plateau where the PCM maintains a nearly constant temperature.

The configuration and its operation suggest the existence of an optimal PCM melting temperature that maximizes the energy stored and transferred to the ORC system. This optimum results from a trade-off. On the one hand, higher melting temperatures enhance ORC efficiency by increasing the working fluid inlet temperature, but they also reduce the amount of heat transferred from the exhaust gases. On the other hand, lower melting temperatures improve heat transfer but penalize ORC efficiency. Therefore, an intermediate melting temperature is expected to yield the highest overall energy recovery.

Fig. 6 illustrates the conceptual benefit of integrating PCM into the WHR system. It presents the frequency-based representation of the exhaust thermal power and the cumulative duration during which each power level is available. The red hatched area represents the energy directly used by the ORC to operate at nominal load. The yellow hatched area indicates the thermal energy that exceeds the nominal requirement and can be stored in the PCM. This stored energy can later be reused to extend the duration of ORC operation at nominal conditions, even when the instantaneous exhaust power is insufficient.

In a conventional WHR system, the ORC can operate only at nominal load when the exhaust thermal power exceeds the required threshold. When the available power drops below this level, the ORC must operate at partial load or shut down, resulting in reduced efficiency and intermittent operation. This limitation reduces the overall energy recovery potential and compromises system continuity.

Thanks to thermal buffering, the PCM-based system allows excess thermal energy to be accumulated during high-power phases and reused during low-power phases. This mechanism extends the duration of ORC operation at nominal conditions, improving overall energy recovery and system stability.

While the integration of PCM offers clear thermodynamic advantages, it also introduces additional mass to the system. This added weight may affect vehicle performance, fuel consumption, and payload capacity. Therefore, a careful trade-off must be made between the

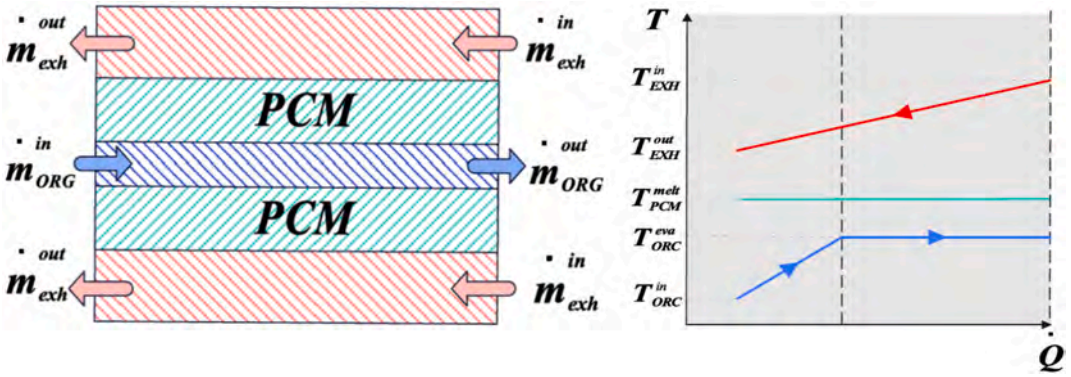

Fig. 5. Schematic of the PCM-based heat exchanger, where the PCM acts as an intermediate thermal buffer between the exhaust gases and the ORC working fluid. Temperature profiles highlight the role of the PCM melting point in regulating heat transfer.

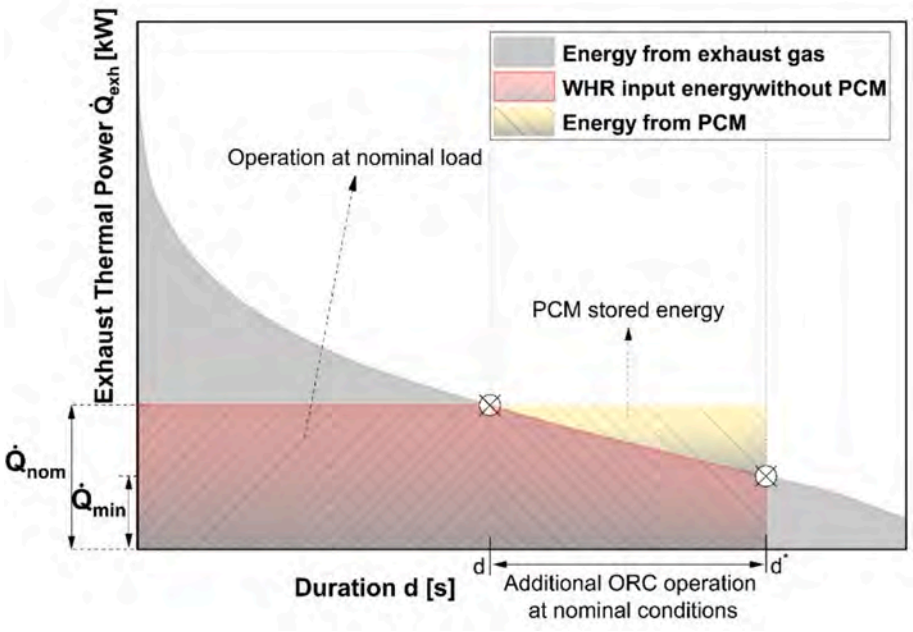

Fig. 6. Frequency-duration diagram for the PCM-based configuration.

thermal benefits of PCM integration and the associated weight penalty. Optimizing the PCM selection, both in terms of material and mass, is mandatory to balance energy storage capacity with system mass and ensure overall efficiency.

To estimate the mass of PCM required, the stored energy is assumed to be related exclusively to the latent heat of fusion, neglecting the sensible heat contribution before and after the phase change. This conservative assumption leads to a slightly higher estimated mass, ensuring a robust design margin. The mass of PCM is computed using the following equation:

$$m_{PCM} = \frac{Q_{stored}}{\lambda} \tag{7}$$

where Q_{stored} is the energy to be buffered (yellow area of Fig. 6), and λ is the latent heat of the PCM. In this quasi-static, upper-bound assessment, PCM sizing prioritizes energy capacity and time extension. Instantaneous charge/discharge rates are not quantified, as they require a dedicated transient model beyond this work's scope.

4. Exhaust gases properties under real-world driving conditions

The temperature and flow rate of a vehicle's exhaust gases change continuously during a trip not only because of dynamic variations in engine load and speed, but also because of variable boundary conditions, such as engine temperature and ambient conditions of temperature, pressure, and humidity. Moreover, the temperature of the exhaust gases decreases along the exhaust line, from the value immediately downstream of the exhaust valve (hot-end) to the tailpipe (cold-end). To obtain realistic information on the variability of exhaust enthalpy, the authors postprocessed the dataset made available by Joubert et al. [20], which contains a comprehensive collection of variables measured on a heavy-duty vehicle (Isuzu FTR 850). The main specifications of the vehicle Isuzu FTR 850 and the engine considered for the investigation are reported in Table 1.

The dataset of Joubert et al. [20] includes 28 trips: the first eight were conducted with the flatbed unloaded, the next 10 with a 1500 kg load, and the last 10 with a 3000 kg load.

However, the temperature values in this dataset refer to the tailpipe, i.e., the cold end of the exhaust line, while the WHR is usually implemented upstream, at an intermediate position between the hot end (engine turbine exit) and the cold end.

To solve this issue, the numerical approach developed and validated in a previous investigation [31] is adopted to determine the temperature at which the gases enter the HEX, which is assumed to be the average of

Table 1
Vehicle and engine specifications.

Vehicle	Isuzu FTR 850
Mass during tests	10740 kg + + payload
Engine	Isuzu 6HK1-TCN
displacement	7.79 L
bore	114.8 mm
stroke	125 mm
number of cylinders	6
Brake power	210 kW @ 1900 rpm
Fuel consumption (H-series)	0.342 lb/HP-h (208 g/kWh)
Transmission and drive	Automated Hydraulic-controlled
number of gears forward	6
gear ratios	{8.51, 4.66, 2.73, 1.78, 1.27, 1.00}
final ratio	5.875
Fuel capacity	400 L
Tires	11 R22.5-16PR (radius 0.52 m)

the hot-end and cold-end temperatures. This temperature will be henceforth defined as T_{exh}^{int} or "intermediate temperature". The validation of the proposed model for trip #4 is shown in Fig. 7. In particular, Fig. 7a shows the dynamicity of the mass flow rate and exhaust temperature with a time-based analysis, while Fig. 6b verifies the accuracy of the model in terms of the frequency distributions of exhaust temperature and mass flow rate. While the thermodynamic model for the ORC system is based on our previously validated work [17], the evaporator model, which establishes the thermal coupling between the engine and the ORC, has been developed specifically for this study. Its formulation and integration are described in detail in the Appendix.

The vehicle model is based on a standard quasi-static approach that was also extended in this investigation to the WHR. This methodology, validated by Villani et al. [28], justifies the use of the two alternative approaches to ORC sizing described in this section: the most frequently operated engine modes and the frequency-duration diagram.

The introduction of the Heat Recovery Vapor Generator into the exhaust gas path increases backpressure and negatively affects engine performance and emissions [28], including Brake Specific Fuel Consumption [30]. The magnitude of this backpressure penalty and its overall impact on system efficiency depend critically on the heat exchanger design and the specific engine characteristics, including the turbocharging strategy [32]. In heavy-duty applications, the achievable output and system design flexibility often allow the net benefit to be maintained or optimized, supporting the hypothesis that the penalty is relatively lower or more acceptable compared to the ORC output. Studies focusing on heavy-duty diesel power generators (1.5 MW, V12) typically investigate backpressure ranges up to 100 mbar [33]. In a heavy-duty truck application, Zhao et al. [34] demonstrated that at high load and high speed (95 km/h, full cargo), the combined penalty (weight and backpressure) is close to 0.71 kW. The same authors quantified the impact of ORC integration on a heavy-duty truck, reporting a power penalty due to system weight of 0.647 kW at 95 km/h, corresponding to 17.1% of the ORC net output at that condition (3.78 kW). Conversely, in low-load scenarios, the recovery potential drops significantly, and the system often operates at zero or negative profit.

In stationary heavy-duty applications, Michos et al. [33] evaluated the effect of ORC evaporator backpressure on a 1.5 MW marine diesel generator. For a recuperated cycle using acetone and a VGT turbocharger, the combined system achieved a 9.8% reduction in BSFC at 50 mbar backpressure. The backpressure penalty reduced the ORC benefit by 10.8%. At 50 mbar, the attenuation was 3.9%.

In their experimental study on a marine diesel engine, Ma et al. [35] reported backpressure-induced power losses of 37.2%, 17.5%, 10.6%, and 10.4% at 100%, 75%, 50%, and 25% loads, respectively. Such losses reduce exergy efficiency, raise brake specific fuel consumption, and increase exhaust exergy waste.

On-road turbocharged HD diesels show lower impacts [36]: typically 1–2%, max 3% at worst point. Design studies confirm ~80 mbar HRVG pressure drop limits fuel penalty to ~0.6% at reference conditions [30]. Our investigation conservatively neglects backpressure effects on exhaust temperature and mass flow. In the proposed system, PCM buffer stabilize ORC operation during transients, while hybridization overcome power loss and efficiency penalty through electric motor assistance, kinetic energy recovery and optimized engine operating points [37].

4.1. Most frequently operated engine modes

In the approach, all trips were aggregated to obtain a global frequency distribution representative of the whole dataset. Since each trip has a drive time of about 1.78 h and the data were sampled with a frequency of 1hz, the whole database corresponds to about 180 thousand operating conditions, comprehensive of different levels of vehicle parameters (speed, acceleration, grade, trailer load), ambient conditions (temperature, pressure, humidity) and engine status (speed, load, coolant temperature, etc.)

The results of the frequency analysis for the 28 trips in the dataset are reported in Fig. 8 as engine operating points. To obtain this distribution, the engine map was segmented into bins measuring 100 rpm by 50 Nm. Then, each bin was color-coded according to how frequently the corresponding torque and speed occurred across all 28 trips. Note that the most frequent engine operating points (indicated by the red bins) are concentrated in the central area of the plot, corresponding to medium–low speeds and very low torque.

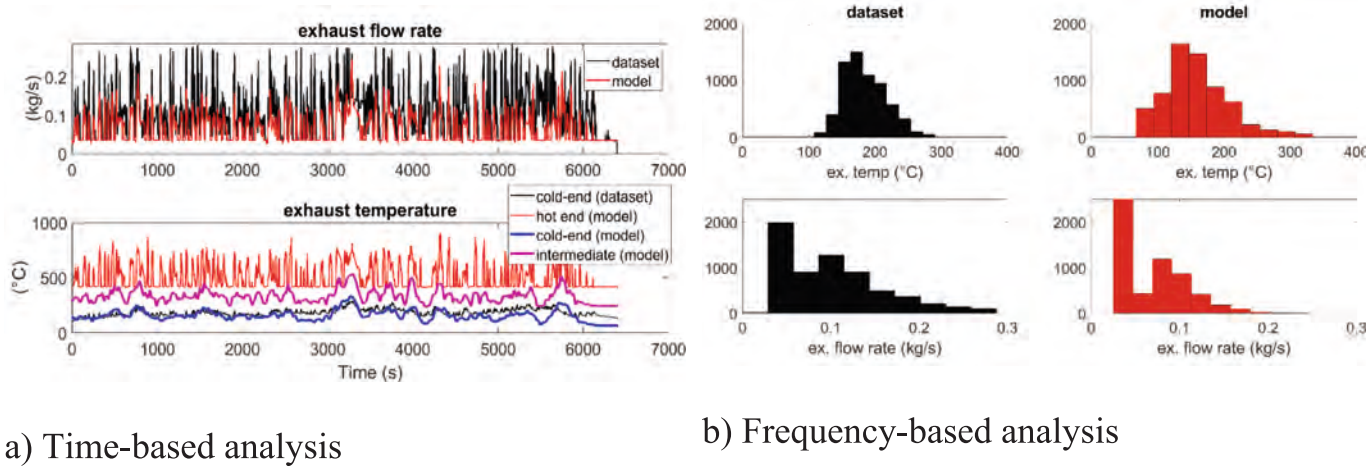

a) Time-based analysis

b) Frequency-based analysis

Fig. 7. Validation of the engine model (trip #4).

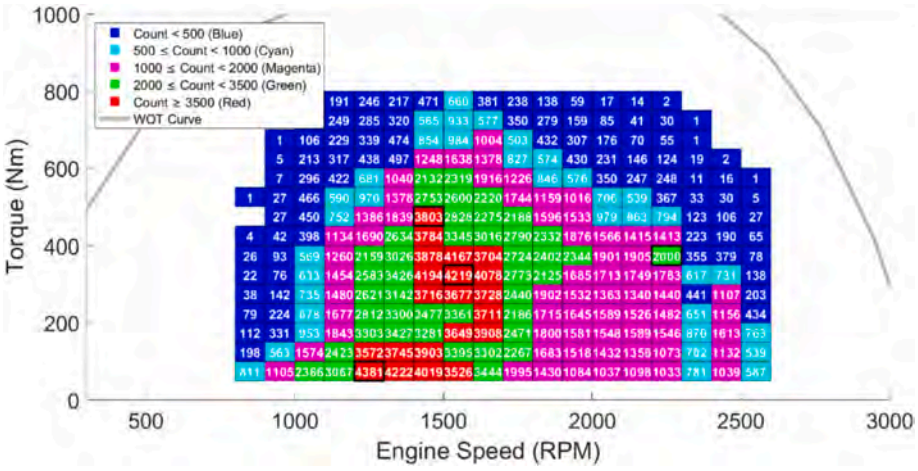

Fig. 8. Results of the frequency analysis and selected modes for the entire dataset.

Four modes were considered for the design of the WHR; their details are listed in Table 2.

The first three modes correspond to the top three most frequent bins of the red region, while the fourth mode was chosen as representative of the high-torque, high-speed region, where the engine exhibits higher exhaust gas temperatures and mass flow rates-conditions that are favorable for sizing the ORC. The fuel flow rate and the engine efficiency reported in Table 2 were obtained from the engine model described in the Appendix.

Fig. 9 shows the distribution of energy flows in the four modes; the exhaust power varies between 25 and 46 percent of the fuel power, while the brake power (*BHP*) is in the range 19–24% of the fuel power. These ranges are consistent with data reported in scientific literature. The thermal power associated with those modes, P_{exh}, was calculated considering the difference between the exhaust temperature and 90°, a typical value registered at the heat exchanger outlet.

The remaining power flows include contributions from heat dissipated through coolant, lubricant oil, mechanical friction, pumping work, and radiation [38]. All these contributions are noted here as $P_{coolant,\cdots}$.

4.2. Frequency-duration diagram

A frequency-duration diagram, similar to that of Fig. 3, was built by cumulating all the thermal power values in the dataset to allow the application of the "maximum rectangle" method to the design of the WHR system. It is important to note that this analysis refers to the thermal power available at the WHR system inlet, not the ORC's net power output.

The analysis can be conducted considering two possible installation positions for the WHR system:

1. At the hot end, where the maximum exhaust temperature, T_{exh} is available;
2. At an intermediate location along the exhaust line, using the estimated values of T_{exh}^{int}.

Table 2
Details of the selected engine modes.

Mode	Symbol	Unit	1	2	3	4
Frequency		–	4219	3803	4381	2000
Engine speed	n_{ICE}	rpm	1550	1450	1250	2250
Engine torque	T_{ICE}	Nm	325	475	75	375
Engine efficiency	η_{ICE}	–	0.22	0.24	0.19	0.21
Fuel flow rate	$\dot{m}_f$	g/s	5.45	6.90	1.22	9.61
Exhaust flow rate	$\dot{m}_{exh}$	kg/s	0.109	0.114	0.059	0.152
Hot-end temperature	T_{exh}	°C	639.1	718.2	462.3	720.3
Intermediate temperature	T_{exh}^{int}	°C	464.1	543.2	287.3	545.3

The first assumption (hot-end) is useful for estimating the maximum theoretical recovery potential of the WHR system, but it is not a realistic installation scenario, especially given its application to biodiesel-fueled engines, which typically have lower exhaust temperatures [39].

The application of the maximum rectangle criterion to the frequency distribution of exhaust thermal power for both temperatures is shown in Fig. 10. The maximum values of power are about 48 kW for the hot-end installation (Fig. 10a), and 21 kW when using T_{exh}^{int}. (Fig. 10b).

These plots also show the rectangles corresponding to the four operating models of Table 2. Note that mode three almost coincides with the optimal value of thermal load when using the intermediate installation (T_{exh}^{int}). This can be explained by noticing that this mode corresponds to the higher value of exhaust energy (see the energy distribution diagrams of Fig. 9).

On the one hand, this indicates an alignment between the two approaches in the more realistic installation scenario, reinforcing the robustness of the sizing strategy. On the other hand, the two methods reflect different perspectives: the mode-based approach identifies the most frequent engine operating point, while the frequency-based method identifies the most persistent thermal power level available for recovery.

To refine the WHR system sizing, the frequency distribution of exhaust gas temperatures was filtered using the compatibility range of the ORC (330 °C −380 °C) identified in Section 3 to ensure thermodynamically viable and operationally safe operation of the ORC. Moreover, a minimum load of 50% was chosen. The updated frequency analysis is shown in Fig. 11 for the realistic case of installation (T_{exh}^{int}); the filtering determines a reduction from 21 kW to 18 kW of the nominal thermal power.

At part load, in the blue area of Fig. 10, the ORC performance was evaluated using the transcritical model described in the Appendix. In the red zone (Fig. 11), no exhaust gas temperature regulation (e.g., via air dilution) is assumed, since the nominal condition can be continuously assured.

5. Results

The optimal power level identified in the previous section, 21 kW, was used to size the ORC plant, based on the Design of Experiments in Table 3, and to determine the optimal configuration. As already stated, the simulations were carried out assuming a maximum working fluid temperature of 250 °C, with the condensation temperature fixed at

Fig. 9. Energy distribution in the selected operating modes.

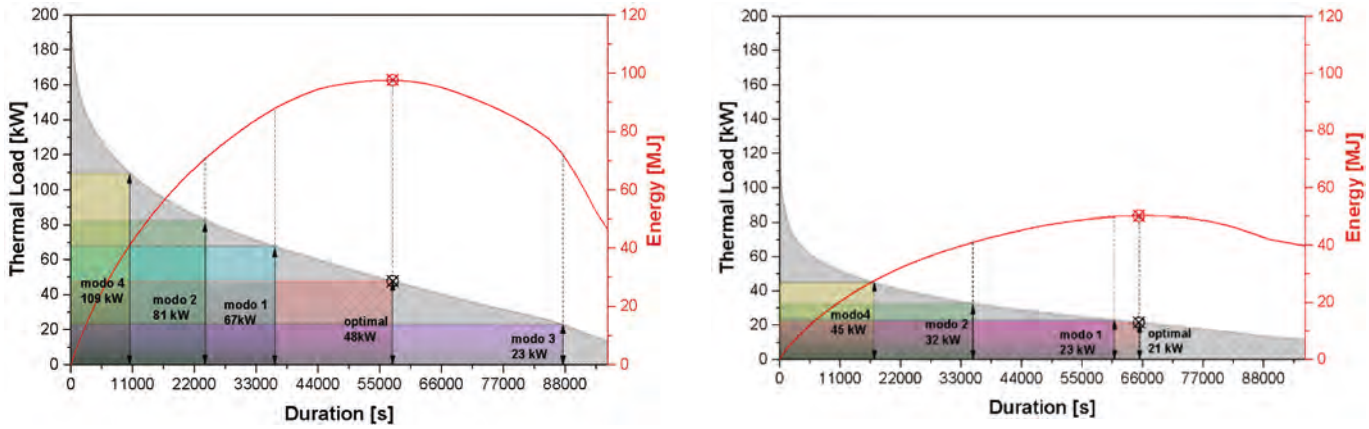

Fig. 10. Power and thermal energy graphs in the frequency domain and most frequent engine operating modes calculated at the hot-end (a) and in the intermediate position (b).

30 °C.

The performance indicators considered for the design of the ORC plant are:

- The net electric power output, P_{ORC};
- The isentropic efficiency of the turbine, $\eta_{is.turbine}$ which reflects the quality of the expansion process.
- The net electric efficiency of the ORC plant, η_{ORC};
- The inlet temperature of the organic fluid to the HRVG, $T_{inlet,of}$;
- The mass flow rate $\dot{m}_{exh}$, i.e., the design mass flow rate of the WHR.
- The minimum acceptable off-design mass flow rate $\dot{m}_{of}$.

5.0.1. *Simple vs IHE*

Fig. 12 shows the thermodynamic cycles with IHE in the T–s diagram for the three selected working fluids, while Table 4 reports the numerical results for both configurations (SIMPLE and IHE) and the three fluids.

Internal regeneration, achieved by preheating the working fluid before it enters the evaporator, clearly outperforms the simple layout in terms of both efficiency and energy recovery, but at the cost of increased complexity and volume.

Among the fluids, R245FA and R1234ZE(E) show comparable performance, while Isobutane, despite a slightly lower net power output, offers advantages in power-to-weight and power-to-volume ratios.

These results provide a preliminary ranking of the working fluids and configurations, which will be further refined through a detailed comparison of heat exchanger sizing and system integration constraints.

5.0.2. *Compatibility with the exhaust gas sources*

A frequency-based evaluation of the exhaust gas mass flow rate was performed using the same experimental dataset from Joubert et al. [20]. This analysis aims to assess how often the exhaust mass flow rate falls within the operating range required by the ORC system, considering the thermal coupling between the exhaust gases and the organic working fluid through the heat exchanger. Mass flow rate data were filtered to exclude conditions unsuitable for heat exchanger operation and minimum load ORC operation.

Fig. 13 shows the results for the R245FA working fluid. Panel (a) shows the time series of experimental data while panel (b) presents the cumulative frequency distribution of the exhaust mass flow rate.

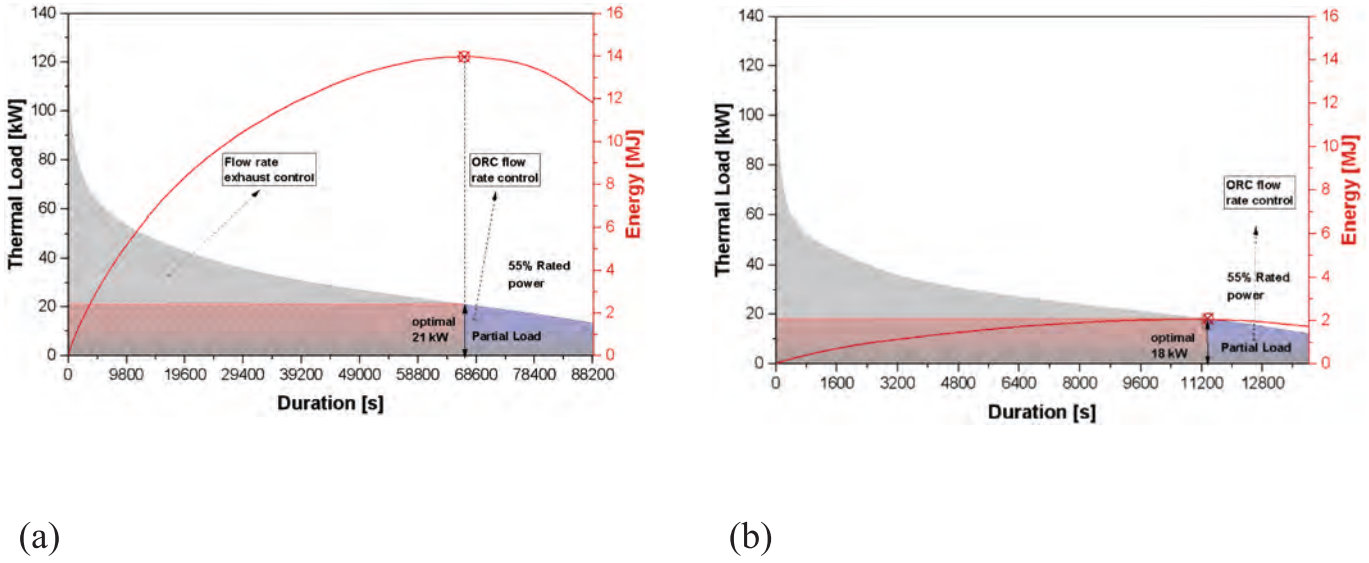

Fig. 11. Power and thermal energy graphs in the frequency domain for unfiltered (a) and filtered (b) temperature.

Table 3
Design of an experiment for the design of the ORC.

Variable	No of levels	Values
ORC cycle	2	Simple, IHE
ORC fluid	3	R245FA, R1234ZE(E), Isobutane
ORC condensation temperature	3	30 °C, 40 °C, 50 °C
Type of HEX	2	Shell and Tube (STHE), Plate (PHE)
Use of PCM	2	Yes, No
PMC material	6	$NaNO_2$, $NaNO_3$,$NaOH$, KNO_3, $LiOH$

Filtering ensures compliance with working-fluid limits and heat exchanger design. The shaded bands in Fig. 13b) indicate the flow rate ranges required for nominal operation of the ORC in both the SIMPLE (blue) and IHE (red) configurations. The comparison shows that the required flow conditions are frequently met in real-world operations, particularly with the IHE configuration, which offers a broader compatibility range. This supports the feasibility of continuous ORC operation and validates the system size based on the selected working fluid.

The contribution of the cooling circuit was excluded from the WHR design because its energy potential is marginal, about 20% of the total engine waste energy. Fig. 14 illustrates this trend: the ratio of coolant energy to exhaust energy always remains between 10 and 20% for the IHE configuration. For the simple configuration, it is always lower than 15%.

In the following analysis, the authors focused exclusively on exhaust heat, ensuring a simpler architecture and a better energy return, which is crucial for heavy-duty applications where packaging and mass constraints are critical.

5.0.3. Plate vs shell and tube HEX

Fig. 15 presents the T–Q diagrams for the three working fluids, R245FA, R1234ZE(E), and Isobutane, using a plate heat exchanger

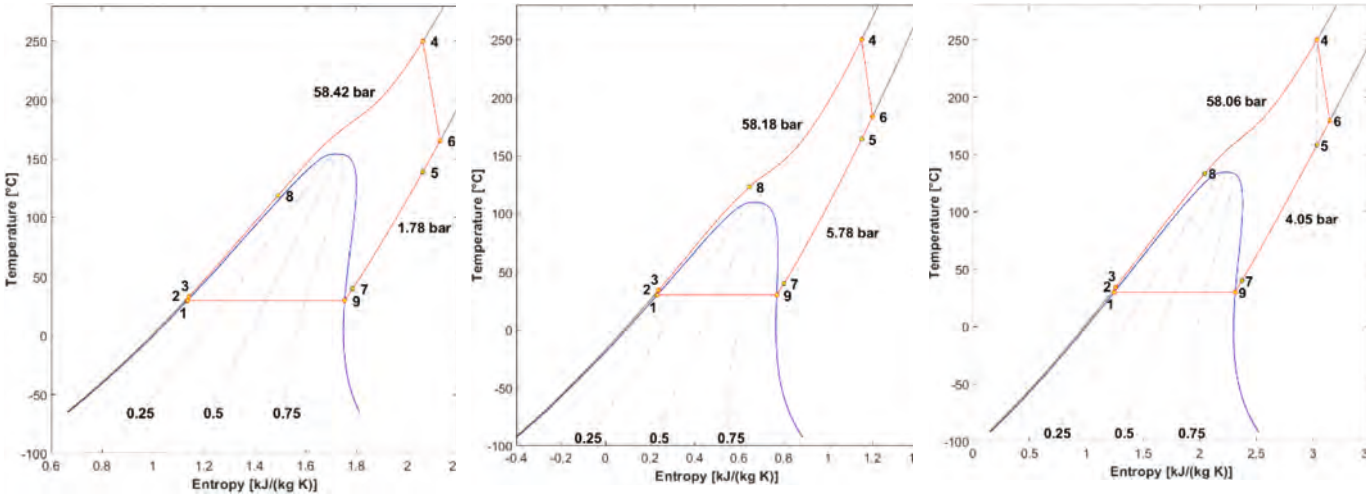

Fig. 12. T-s diagrams and thermodynamic cycle of the IHE system at 250 °C maximum temperature and 30 °C condensation temperature for the fluids (a) R245FA, (b) R1234ZE, and (c) ISOBUTANE.

Table 4
Main performance indexes for the configuration analyzed. $T_{max,ORC} = 250^{\circ}C, Q_{th,in} = 18kW, T_{cond} = 30^{\circ}C, P_{nom} = 1.6*P_{critical}$.

	ISOBUTANE		R245FA		R1234ZE	
Type	SIMPLE	IHE	SIMPLE	IHE	SIMPLE	IHE
$\dot{m}_{exh}(kg/s)$	0.067	0.085	0.0696	0.079	0.0696	0.081
$\dot{m}_{of}(kg/s)$	0.024	0.0384	0.0473	0.067	0.0487	0.077
$P_{ORC}(kW)$	1.78	2.98	2.02	3.01	1.59	2.79
$\eta_{is.turbine}$	0.599	0.622	0.604	0.621	0.595	0.618
η_{ORC}	0.103	0.175	0.116	0.179	0.093	0.161
$T_{IHE.inlet}$	32.8	135.8	32.8	121.6	32.8	124.4

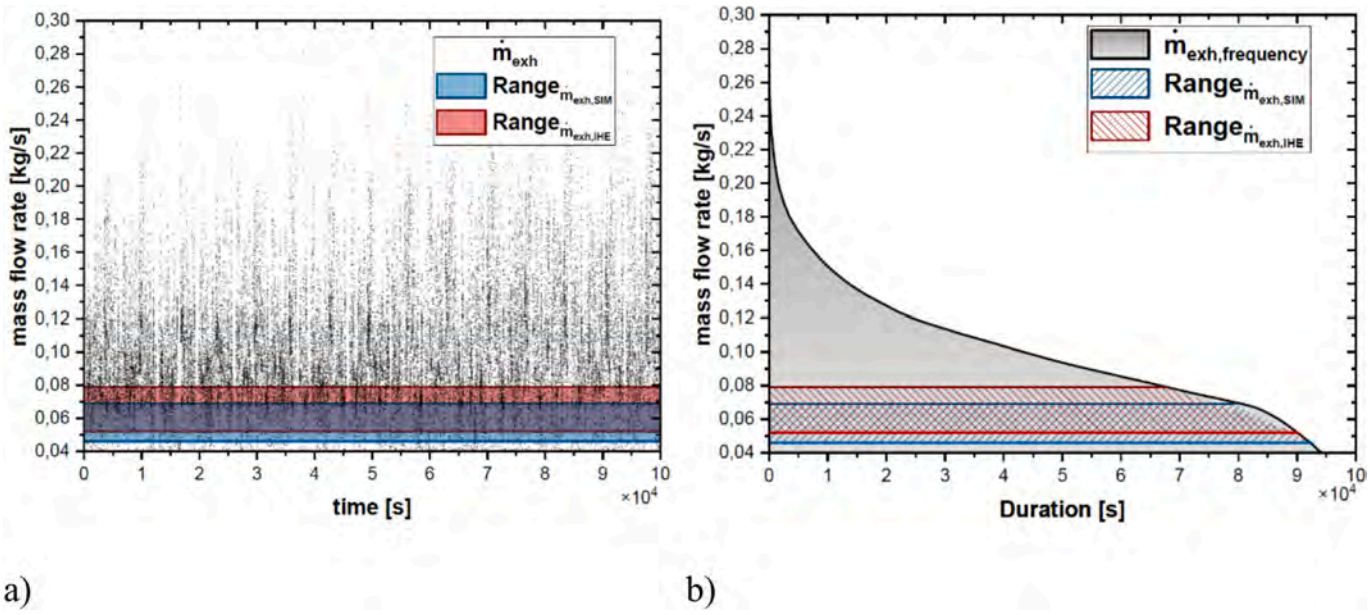

Fig. 13. Exhaust mass flow rate frequency diagram for WHR configuration operating with R245FA.

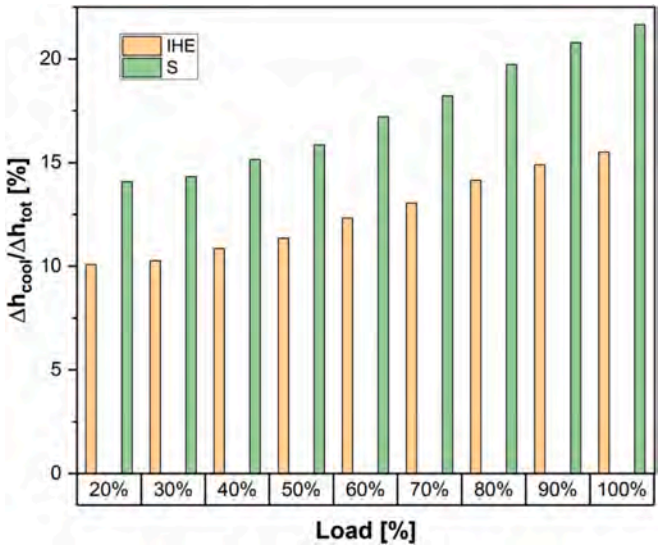

Fig. 14. Contribution of the energy available to the coolant circuit compared to the exhaust recoverable energy for simple and IHE configurations across torque levels (partial load conditions).

(PHE). These plots illustrate the thermal interaction between the exhaust gases and the organic fluid along the heat exchanger. The shape of the curves reflects the thermophysical behavior of each fluid, particularly during the isothermal evaporation phase. The slope and length of the isothermal segment vary among the fluids, indicating differences in latent heat and heat transfer effectiveness. Notably, the regenerative configuration (IHE) results in a higher inlet temperature to the evaporator, shifting the evaporation plateau and improving thermal matching with the exhaust stream.

Table 5 and Table 6 report the performances of the heat exchangers for the plate (PHE) and shell-and-tube (STHE) configuration, respectively, while their geometrical specifications are reported in the Appendix.

In both cases, the IHE layout requires a larger heat transfer area due to the increased energy recovery and the higher inlet temperature of the working fluid $T_{out,exh}(^{\circ}C)$. The PHE configuration offers higher thermal effectiveness, η_{HX}(up to 92.6%) and more compact dimensions, making it suitable for space-constrained applications. Conversely, the STHE design, while slightly less efficient, provides greater mechanical robustness and is better suited for high-pressure operation.

5.0.4. Choice of the PCM and integration in the WHR system

As introduced in the methodology, the innovative PCM-based heat exchanger relies on the phase change material as an intermediate thermal buffer between the exhaust gases and the ORC working fluid. Since the PCM operates most effectively during its melting phase, selecting its melting temperature is a key design parameter. An innovative contribution of this work is the optimization of the PCM melting temperature to maximize the energy storage potential of the WHR system.

Fig. 16 illustrates the thermal energy stored by the PCM-based heat exchanger as a function of the PCM's melting temperature, aiming to identify an optimal value that maximizes energy recovery. This optimal

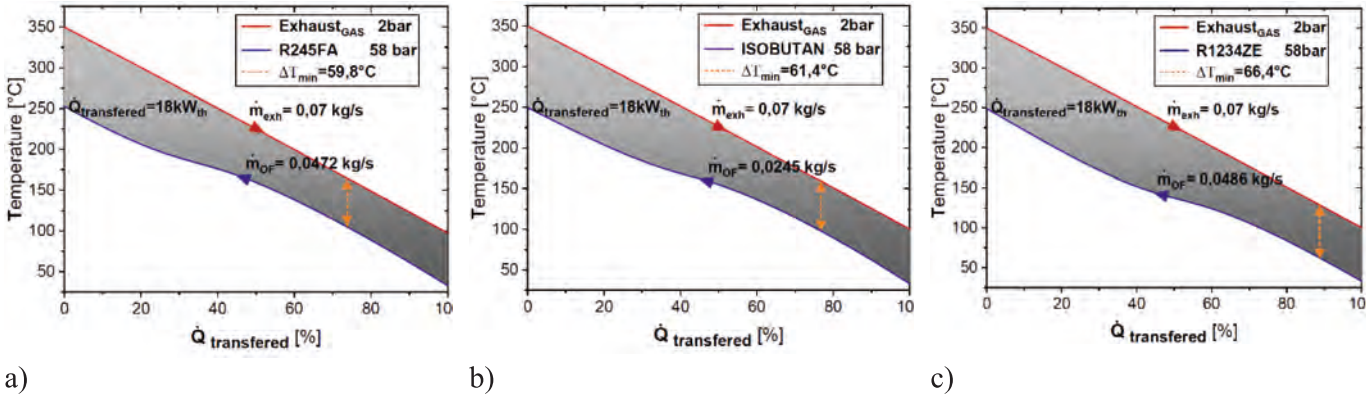

Fig. 15. T–Q diagrams for the three working fluids—R245FA, R1234ZE(E), and Isobutane—using a plate heat exchanger (PHE).

Table 5
Performance of plate heat exchangers.

Type	ISOBUTANE SIMPLE	IHE	R245FA SIMPLE	IHE	R1234ZE SIMPLE	IHE
Heat transfer area (m^2)	0.185	0.201	0.205	0.259	0.187	0.238
$T_{out.of}$ (°C)	249.6	249.4	249.9	250	248.93	249.8
$T_{out.exh}$ (°C)	100.9	156.7	100.4	140.4	100.3	144.6
η_{HEX}	79.5	91.1	79.5	92.6	79.5	91.9
U (W/m^2K)	1509.3	1670.3	1062	1360.2	1158.4	1143.4

Table 6
Performances of conventional shell and tube heat exchangers.

	ISOBUTANE		R245FA		R1234ZE	
Type	SIMPLE	IHE	SIMPLE	IHE	SIMPLE	IHE
Heat transfer area (m^2)	0.359	0.41	0.382	0.44	0.358	0.42
$T_{out.of}$ (°C)	250.6	250.0	249.2	249.4	251.6	247.2
$T_{out.exh}$ (°C)	99.2	156.6	98	144	101.47	148.2
η_{HEX}	79	90.5	79.2	89.8	78.3	89.6
U (W/m^2K)	617.9	834	570.1	735.5	606.6	730.7

result arises from a trade-off between two opposing effects. As the melting temperature increases, the ORC efficiency initially improves due to higher fluid inlet temperatures. On the other hand, higher melting temperatures reduce the amount of energy transferred from the exhaust gases to the PCM, since the exhaust temperature must remain above the melting point to enable heat transfer.

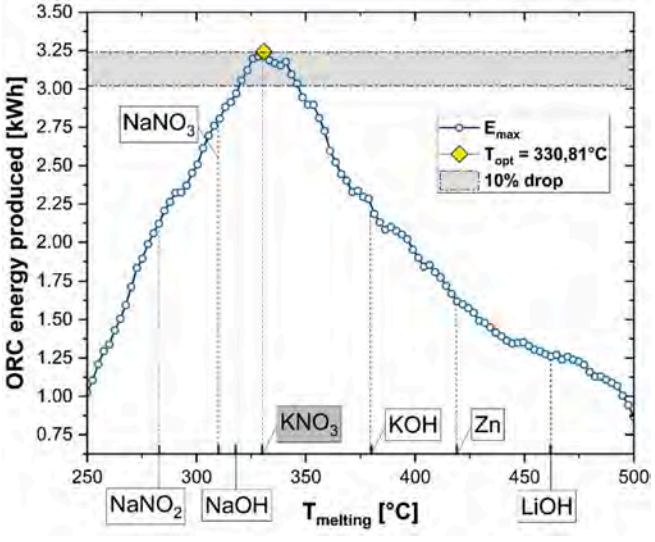

Fig. 16. Optimization of PCM Melting Temperature for Maximum Energy Recovery.

The curve in Fig. 16 shows that the optimal melting temperature, marked by a yellow diamond, is 330.8 °C and corresponds to a maximum stored energy of approximately 3.2 kWh. A shaded grey band highlights the region where the stored energy remains within 10% of the optimum, indicating a practical range of melting temperatures with minimal performance loss.

To assess the feasibility of this optimum, seven existing PCM materials are considered and positioned along the x-axis. $NaNO_3$ ($T_{melt} \approx$ 330 °C) lies almost exactly at the optimal point, making it an excellent candidate. NaOH ($T_{melt} \approx$ 320 °C) and KNO_3 ($T_{melt} \approx$ 340 °C) fall within the 5% loss zone, showing strong potential for practical application. Finally, $NaNO_2$ ($T_{melt} \approx$ 280 °C), KOH ($T_{melt} \approx$ 380 °C), Zn (≈420 °C), and LiOH ($T_{melt} \approx$ 450 °C) are further from the optimum and outside the grey zone, suggesting lower suitability for this specific configuration.

Fig. 17 illustrates how the energy stored in the PCM allows the ORC to operate continuously at nominal load, even during periods when the exhaust thermal power falls below the design threshold. In particular, the yellow-shaded area of Fig. 17 represents the additional energy buffer required to maintain nominal ORC operation across all 28 driving cycles. The total energy to be stored is approximately 7562 kJ, which corresponds to the cumulative deficit between available and required thermal power. This energy can be stored during high-load phases and released during low-load intervals, effectively smoothing the thermal input to the ORC and extending its operating time at optimal efficiency.

Note that the frequency distribution of thermal power appears truncated at lower values, likely due to limitations in the dataset. In real-world scenarios, the curve would be expected to decay more gradually toward zero. This implies that the PCM-based configuration could offer even greater benefits in extending ORC operation under partial-load conditions by recovering residual thermal energy that is currently unaccounted for in the current analysis.

It is also important to note that the performance enhancement provided by PCM-based configurations could be even more significant in subcritical ORC systems. In these systems, the efficiency drop under partial load conditions is typically more pronounced than in transcritical

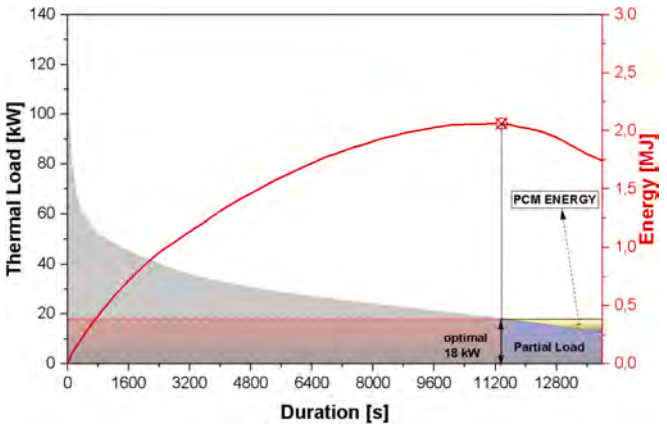

Fig. 17. Sizing of the WHR system based on PCM heat exchangers.

cycles. Therefore, the ability of PCMs to extend nominal operation by buffering excess thermal energy becomes even more valuable. Although this study focused on transcritical ORC architectures to explore the highest performance potential, the results suggest that PCM integration may offer even greater benefits in subcritical applications, where the efficiency decay with load is steeper and the recovery of residual energy is more critical.

The seven PCMs are compared in Table 7 in terms of melting temperature (T_{melt}), latent heat (λ), and thermal conductivity. Moreover, it shows the mass of PCM required for different materials to store the exhaust energy made available by the exhaust gases. For instance, 28 kg of KNO_3, a salt with a melting point close to the optimal value (Table 7), would be sufficient to store the required energy. In contrast, materials with lower latent heat, such as potassium hydroxide (KOH), require up to 50 kg to achieve the same storage capacity. In addition to mass, the required volume of PCM varies significantly across the analyzed materials. The estimated volume ranges from about 13.5 L for KNO_3 to nearly 25 L for KOH. $NaNO_3$ and NaOH fall in an intermediate range (around 19–21 L), highlighting the importance of considering packaging constraints alongside thermal performance. This highlights the importance of selecting a PCM with both a suitable melting temperature and high latent heat.

This PCM-based strategy complements the previous findings on ORC performance and heat exchanger sizing. While the IHE configuration already improves efficiency by increasing the fluid inlet temperature, the PCM buffer further enhances system robustness by decoupling the ORC from the instantaneous variability of the exhaust source. This is particularly valuable in real-world driving conditions, where thermal input fluctuates rapidly.

In summary, the PCM selected for the present design is potassium nitrate (KNO_3), identified through a melting temperature optimization with an optimal melting temperature of 330.8 °C (Fig. 16). For ease of reference, the key properties and sizing figures are highlighted in Table 7; required PCM mass and volume are 28.4 kg and 13.5 L, respectively.

Table 7
Properties and required mass of candidate phase change materials.

PCM	Melting temperature [°C]	Latent heat [kJ/kg]	Conductivity [W/(mK)]	Density [g/cm^3]	PCM weight [kg]
$NaNO_2$	283	212	–	2.168	–
$NaNO_3$	310	172	0.5	2.257	43.9
KNO_3	**330**	**266**	**0.5**	**2.109**	**28.4**
NaOH	318	165	0.9	2.130	45.8
KOH	380	150	0.5	2.044	50.4
LiOH	462	873	–	1.460	–

5.0.5. *Effect of condensation temperature on part-load behavior*

A parametric analysis across different condensation temperatures highlights the sensitivity of ORC performance to ambient conditions, offering useful guidance for control strategy and component sizing, especially in applications such as the automotive sector, where ambient temperature fluctuations are significant. In fact, to minimize weight and complexity, vehicle ORC systems typically adopt air-cooled condensers. Performance is thus evaluated at fixed condensing-temperature set-points in a quasi-static framework (i.e., constant condensing temperature under off-design conditions) [27].

points when the condensation temperature increases from 30 °C to 50 °C.

Three condensation temperatures (30, 40, and 50 °C) were considered, with a maximum cycle temperature fixed at 250 °C. Fig. 18 shows electrical and thermal efficiency versus load for both Simple and regenerative configurations, highlighting the impact of condensation temperature. The minimum modeled load is about 60%, imposed by transcritical operation and pressure constraints (≈1.03 times the critical pressure [40]). Both simple and IHE configurations exhibit similar trends, but IHE shows a nearly uniform upward shift in electrical efficiency. The results show that increasing the condensation temperature from 30 °C to 50 °C reduces electrical and thermal efficiency at the design load in a similar manner across all conditions and configurations analyzed. Raising the condensation temperature from 30 °C to 50 °C penalizes both electrical and thermal efficiency across all configurations.

For brevity, let us consider R245 as the working fluid. For the Simple arrangement, electrical efficiency rises slightly with load, from about 11.6% at minimum load to 12.7% at full load for the minimum condensation temperature (30 °C). Furthermore, it drops to 9.8% (minimum load) and 10.6% (full load) at 50 °C condensation temperature. Thermal efficiency follows the same pattern, decreasing by roughly 2.5 percentage.

On the other hand, the IHE configuration consistently improves electrical efficiency across the load range, reaching up to 19.2% at full load, with gains of about 6.5 points compared to the simple one, while slightly reducing thermal efficiency (2 points). This advantage remains stable even at higher condensation temperatures, confirming the effectiveness of regeneration in improving electrical performance. The improvement is nearly uniform across the load band, achieved with the addition of a single component, i.e., the internal heat exchanger. These results confirm robust operation over the range; efficiency decreases with higher condensation temperature, but viable performance is maintained up to 50 °C—even under air-cooled onboard conditions.

5.1. *Global performance and comparison*

This section provides a comparative overview of the global performance indicators for WHR configurations, both conventional and innovative, with phase change material integration. Fig. 19 and Fig. 20 show the final aggregated performance indicators over the entire set of real-world driving cycles: overall WHR system efficiency, ORC thermal efficiency, and the heat source utilization factor.

Fig. 19 refers to the six traditional ORC configurations (i.e., without PCM). For each configuration, a triplet of bars represents the three key performance indicators. The regenerative WHR arrangement operating with R245FA achieves the highest ORC thermal efficiency (17.59%) and WHR efficiency (10.55%), while maintaining a utilization factor above 96%. The nominal power of the system found through the maximum rectangle method described reaches the highest value (3.1 kW). This confirms the effectiveness of internal regeneration in enhancing cycle performance, especially under variable thermal input conditions. The utilization factor values are always close to 96% across all configurations, indicating that the traditional systems are almost constantly active and able to process thermal energy from the exhaust gases throughout the driving cycles, thanks to their effective part-load capabilities.

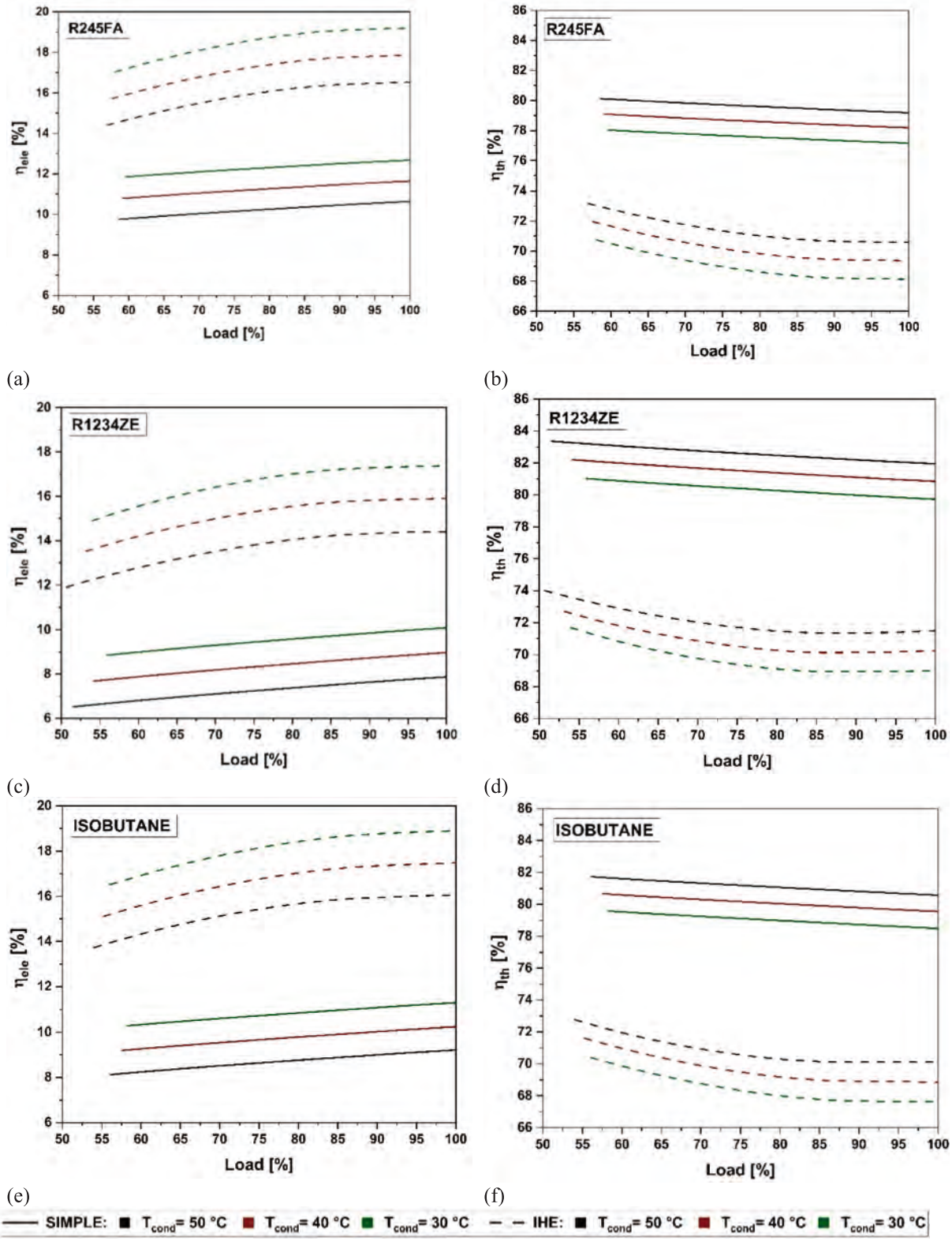

Fig. 18. Electrical and thermal efficiency at partial load of the TORC system in Simple and IHE configuration for the fluids R245FA, R1234ZE, and ISOBUTANE at 250 °C.

When the PCM-based heat exchanger is introduced (Fig. 20), all configurations show a slight improvement in both ORC and WHR efficiencies. The regenerative R245FA system achieves ORC and WHR efficiencies of 18.54% and 11.35%, respectively, an increase of nearly one percentage point over the non-PCM case. This gain is attributed to PCM's ability to store excess thermal energy during high-load phases and release it during low-load intervals, thereby extending the duration of nominal ORC operation and reducing the frequency of partial-load conditions. The utilization factor reaches 97% for the PCM-based configuration, indicating that PCM integration enhances the quality of

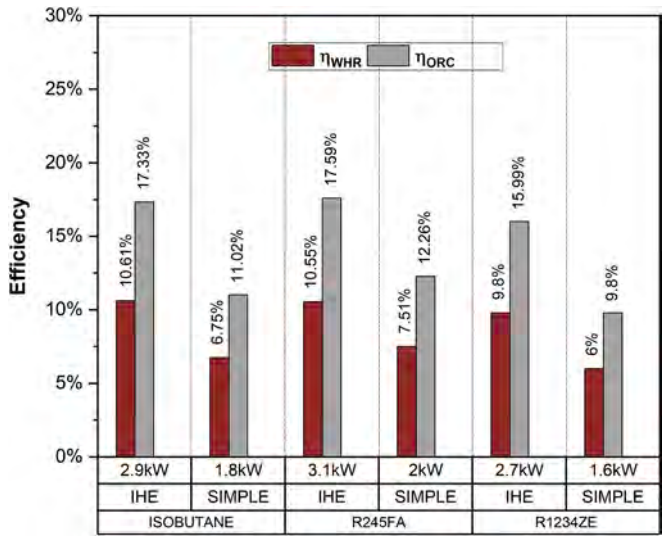

Fig. 19. Electrical and thermal efficiency at partial load of the ORC system for the simple configuration for the fluids R245FA, R1234ZE, and ISOBUTANE at 250 °C (no PCM).

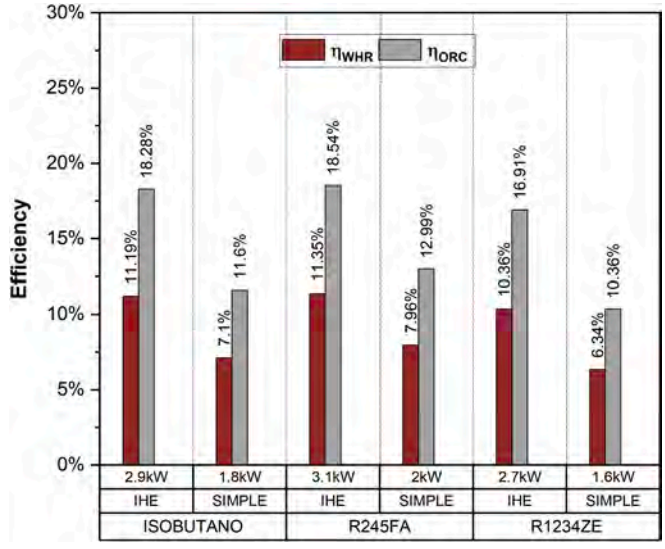

Fig. 20. Electrical and thermal efficiency at partial load of the TORC system in the IHE configuration for the fluids R245FA, R1234ZE, and ISOBUTANE at 250 °C (with PCM).

energy conversion by stabilizing the thermal input.

Overall, the bar plots highlight the synergistic benefit of combining regenerative ORC architecture with PCM-based thermal storage. This approach not only improves energy recovery but also supports more robust and efficient operation under real-world driving conditions, aligning with the broader goals of the IRIDESCENT project.

5.1.1. Impact of PCM addition on the vehicle

The power-to-weight ratio (PWT) of ORC systems vary considerably due to multiple design parameters, including the choice of working fluid, the specific system configuration, and, notably, the condensation temperature. These factors collectively influence the size and mass of key components, particularly the heat exchangers. Among the various fluids examined in the literature, R245fa has emerged as one of the most widely adopted in automotive applications, thanks to its favorable thermodynamic properties and compatibility with compact ORC layouts. According to the data reported by Pili et al. [41], for ORC systems operating with R245fa, the estimated unit weight ranges from approximately 17.3 kg for a 2 kW system to 34.9 kg for a 4 kW system. In addition to the ORC unit weight (17–35 kg for 2–4 kW class, consistently with power-to-weight results in long-haul trucks), the optimized PCM selection (KNO_3) adds 28.4 kg, yielding a total mass of about 58 kg for the analyzed case. Vehicle-scale ORCs reported in the literature reach masses around one hundred kilograms (e.g., ~129 kg in heavy-duty truck studies [14]), which frames the present design toward the lower end of typical vehicular additions [14,42].

6. Limitations of the present work and future directions

Vehicle-scale Organic Rankine Cycle (ORC) systems typically induce exhaust backpressure in the range of 5–20 kPa (corresponding to a 2–4% engine power penalty), and face significant packaging constraints in the vicinity of turbochargers, DPF, and SCR units. These aspects are not explicitly addressed in the present investigation. Indeed, experimental studies on automotive ORCs rarely report system mass, exhaust backpressure, and installation constraints in a comprehensive and consistent manner. Among the available contributions, Soldado et al. [43] provide one of the most complete vehicle-scale assessments by simulating heavy-duty truck ORC systems equipped with axial turbines and using R134a as the working fluid. Their study reports fuel consumption reductions of 2–10% over NEDC and Artemis cycles and discusses packaging limitations; however, system mass and backpressure are not experimentally quantified and are instead inferred through GT-Power simulations. Sun et al. [44] experimentally investigated a 3 kW laboratory-scale ORC prototype under steady-state conditions, achieving efficiencies between 3 and 9.6% and highlighting the sensitivity to condensation temperature, but without addressing vehicle-level integration. Similarly, Srivastava et al. [45] developed a 10 kW turbine, yet vehicle integration aspects were not considered. Recent five-year review papers focused on internal combustion engine applications further confirm the limited number of fully built automotive ORC prototypes and emphasize space-driven constraints as a key barrier. These surveys also highlight the need for a deeper understanding of the impact of waste heat recovery (WHR) unit backpressure on overall engine performance, calling for dedicated assessments [46]. In light of these limitations, the present study adopts a feasibility-oriented perspective, relying on literature-based ranges for system mass and exhaust backpressure. Future work will extend the analysis to a targeted techno-economic assessment of the transcritical layout, with particular attention to the implications of increased maximum pressure and component complexity. This will allow identifying operating conditions under which the performance gains associated with higher cycle pressures and temperatures justify the additional costs in heavy-duty vehicle applications.

The present investigation is further limited to steady-state operating conditions and does not address the dynamic response of the ORC system to variations in the hot source. This choice is consistent with the main objective of the paper, namely the assessment of the thermodynamic performance of an ORC-based waste heat recovery system at representative engine operating points, and with common practice in the literature. Incorporating thermal and mechanical inertia effects, as well as transient interactions between exhaust gases and the ORC loop, would require a fully dynamic modeling framework based on time-dependent mass and energy balances and detailed information on engine geometry, operating strategies, control logic, and exhaust gas pulsations. Such data are not available for the literature-based engine considered in this study. Under these conditions, a simplified transient analysis could yield misleading results. Accordingly, the steady-state approach adopted here is sufficient to identify achievable performance levels and to compare the proposed ORC configuration against alternative solutions. Future developments will therefore focus on a comprehensive dynamic modeling of the entire waste heat recovery system, including both the ORC loop and the tailpipe. This activity will be conducted using a different engine for which detailed geometrical, operational, and control data are available, enabling a consistent and

physically meaningful assessment of transient behavior.

Finally, this design-oriented modeling study does not address thermal-cycling durability, corrosion and compatibility issues, or the long-term stability of the selected phase change material (PCM), namely KNO_3. While nitrate-based PCMs such as $KNO_3/NaNO_3$ are generally less aggressive than chlorides, they require strict control of moisture and impurities; for instance, unprotected $NaNO_3$ has been reported to lose up to 12% of its latent heat over repeated cycles, a degradation that can be mitigated through encapsulation or composite formulations [47,48]. More aggressive PCMs, such as NaOH, demand corrosion-resistant containment specifically designed for high-temperature molten salt environments [49]. Addressing these aspects requires component-level experimental investigations at higher technology readiness levels under vehicle-representative exhaust conditions. Such efforts are beyond the scope of the present work and are being addressed separately in a dedicated PCM literature survey currently under development by the authors.

7. Conclusions

The investigation described the design process and off-design analysis of an advanced WHR system that exploits the exhaust gas of a compression-ignition thermal engine in a heavy-duty vehicle. In particular, a quasi-static frequency-based analysis was performed on 28 real-world driving cycles to determine the most persistent thermal power levels available from exhaust gases. The heat exchanger model used to evaluate the thermal power input to the ORC was validated against reference data from literature. Simulation outcomes confirmed the model's accuracy against reported results, with relative errors below 3%, indicating its suitability for supercritical ORC applications. A key innovative contribution of this work was the optimization of the PCM melting temperature to maximize the energy storage potential of the WHR system. The analysis considered two methodologies for exhaust gas frequency analysis, two locations for the WHR, different configurations, fluids, and operating conditions of the ORC plant, two types of HEX, and seven options for selecting the PCM.

The main findings of the present work are the following:

- The frequency analysis of the engine's thermal output for ORC sizing, using the "maximum rectangle" criterion and the most-frequent engine operating modes, resulted in very close values: 21 kW and 23 kW, respectively.
- The parametric analysis of the ORC unit under nominal and partial-load conditions highlighted the best performance of the regenerative configuration, which yielded gains of 5.3–6.7 percentage points in electrical efficiency and 3.0–4.1 points in thermal efficiency compared to the simple layout. For R245FA, the penalty from increasing condensation temperature from 30 °C to 50 °C was quantified: electrical efficiency dropped by 2.2 points at design load and 3.4 points at minimum load.
- The PCM analysis identified an optimal melting point of 330.81 °C, corresponding to a stored energy of 3.2 kWh. Based on this result, potassium nitrate (KNO_3) was selected as the most suitable material, requiring only 28.4 kg to store the necessary 7562 kJ of thermal energy. This enables the ORC to maintain nominal operation even during low exhaust power phases, significantly enhancing system robustness and energy recovery.
- The PCM optimization analysis, along with the ORC parametric investigation, was used to calibrate the WHR model for global performance evaluation. The regenerative configuration consistently outperformed the simple cycle arrangement. For example, the conventional recovery unit operating with R245FA increased the global efficiency from 7.51% to 10.55%.
- The integration of PCM into the heat exchanger significantly extended the operational range of the ORC system, with a significant improvement in performance, raising ORC efficiency to 18.54% and WHR efficiency to 11.35%, and achieving a utilization factor exceeding 96% in all cases.

Note that the potential benefit of PCM integration could be even greater in terms of global performance improvement in subcritical ORC systems. In fact, such systems are characterized by sharper efficiency drops under partial load, and the ability of PCM to extend nominal operation could become even more valuable. Under transcritical operation, the working fluid temperature increases continuously along the heater, without an isothermal evaporation plateau. As a result, the evaporator operates with smaller temperature differences and maintains higher effectiveness over a wider load range. In contrast, subcritical configurations include an isothermal phase-change section, leading to larger temperature gradients between the heat source and the working fluid. Based on experimental ORC data reported by Jiménez Arreola [50], the efficiency at approximately 80% load reaches about 95.48% of the nominal value for a subcritical cycle, whereas the corresponding transcritical configuration (R245fa as the working fluid, IHE arrangement, condensation temperature of 30 °C) retains roughly 97.61% efficiency. This difference of about 2.1 percentage points is non-negligible. Accordingly, the integration of a phase change material (PCM) unit upstream of the HRVG can provide comparatively larger benefits in subcritical layouts, since the more pronounced efficiency degradation at part load leaves a greater fraction of recoverable heat available for storage and subsequent release during periods of reduced source availability.

In conclusion, this investigation demonstrates that integrating regenerative ORC architecture with PCM-based thermal storage enables a compact, efficient, and robust utilization of exhaust-gas thermal energy to generate on-board electricity. Therefore, the validated methodology and quantified performance indicators provide a solid foundation for future activities of the IRIDESCENT project, which involve applying the methodology to hybrid biodiesel-electric heavy-duty vehicles and executing a system-level optimization.

CRediT authorship contribution statement

Pietropaolo Morrone: Writing – review & editing, Writing – original draft, Validation, Supervision, Software, Methodology, Investigation, Funding acquisition, Data curation, Conceptualization. **Paolo Cutuli:** Writing – original draft, Resources, Methodology, Investigation, Data curation. **Talha Mujahid:** Writing – review & editing, Validation, Formal analysis. **Angelo Algieri:** Writing – review & editing, Formal analysis. **Luigi Falbo:** Validation, Supervision, Data curation. **Teresa Donateo:** Writing – review & editing, Project administration, Methodology, Funding acquisition, Formal analysis.

Declaration of competing interest

The authors declare that they have no known competing financial interests or personal relationships that could have appeared to influence the work reported in this paper.

Acknowledgments

We acknowledge financial support under the National Recovery and Resilience Plan (NRRP), Mission 4, Component 2, Investment 1.1, Call for tender No. 1409 published on 14.9.2022 by the Italian Ministry of University and Research (MUR), funded by the European Union – NextGenerationEU – Project Title IRIDESCENT – P2022YB8HY CUP F53D23009880001 - Grant Assignment Decree No. 5 adopted on 01/09/2023 by the Italian Ministry of University and Research (MUR).

Appendix

This appendix describes in the details the quasi-static modeling of the engine and the modeling approach used for the WHR.

7.1 Prediction of the exhaust gases temperature and mass flow rate under real-world driving conditions

A backward quasi-static simulation approach with a discretization of 1s was adopted for the simulation of the conventional thermal power system of the Isuzu FTR850. At each step, the vehicle speed and road grade profiles are used to calculate the traction force $F_t(i)$ and the required engine power $P_T(i)$

$$P_{ICE}(i) = f\begin{cases} \dfrac{F_t(i)V(i)}{\eta_{gb}} + P_{aux}, V(i) > 0 \\ P_{aux}, V(i) \leq 0 \end{cases} \tag{8}$$

In this equation, $\bullet\eta_{gb}$ is the overall efficiency of the drivetrain while P_{aux} is the parasitic power of the auxiliaries. The engine operating point is then estimated using the value $rpm(i)$ from the dataset and the required power of eq. (8) and used to enter the maps of exhaust mass flow rate and temperature (hot-end). To account for the thermal loss and inertia in the exhaust line, the temperature at the cold-end was obtained by subtracting 350°C independently from the engine load and speed and applying a moving window filter. The value of 350°C was identified from the matching of experimental data for trip #4 and the applied to all other trips. An intermediate temperature was calculated as the average between the other two. The estimation of the cold-end and intermediate temperature is performed by the block "exhaust system model" of Fig. 21. The development of the engine maps and the validation of the whole modeling approach can be found in [51]. Future works will address the effect of ORC integration in heavy-duty engines, focusing on higher exhaust energy and operational stability, to quantify and mitigate the impact of backpressure and additional weight, and the adoption of biofuel instead of fossil diesel.

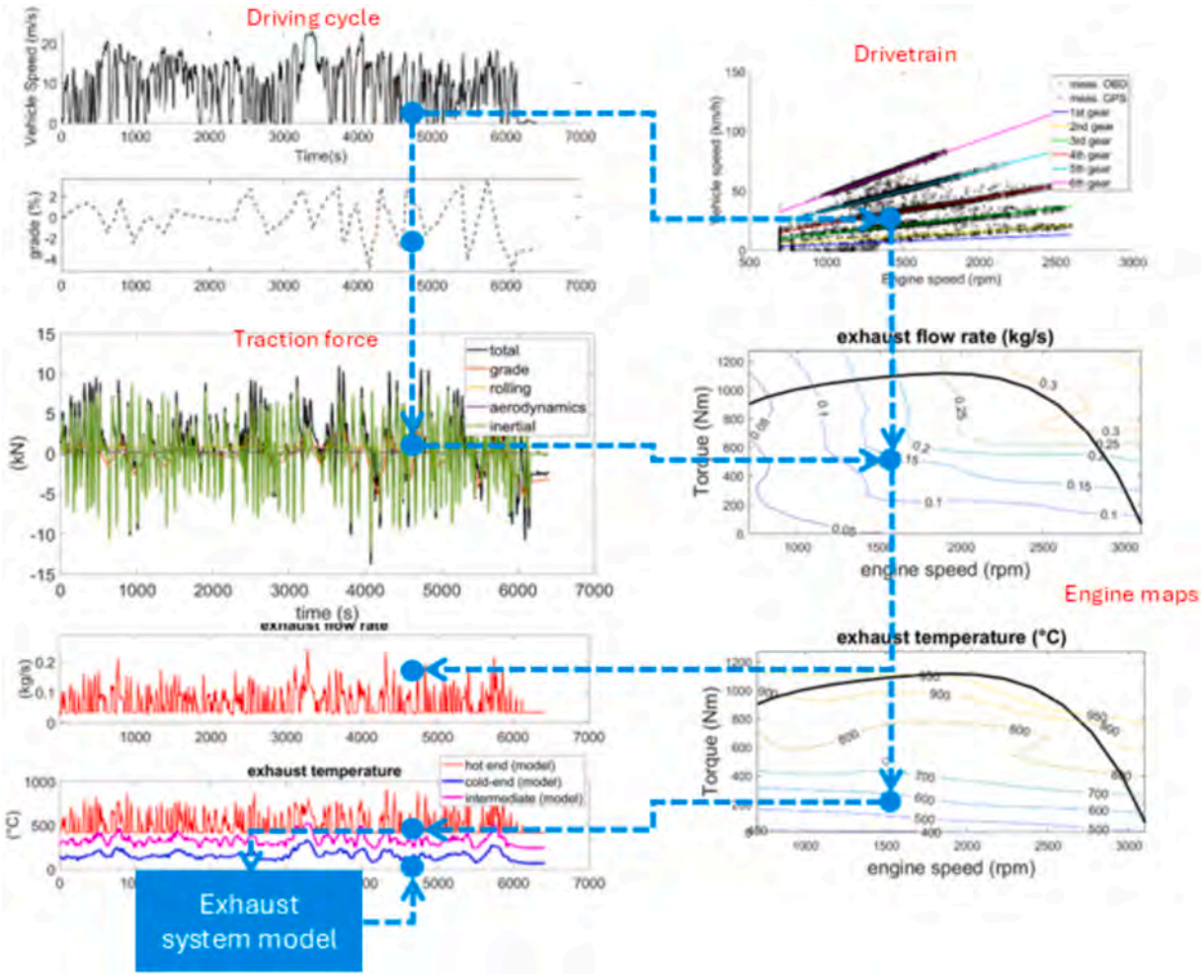

Fig. 21. Flowchart of the modeling approach.

7.2 ORC Thermodynamic model

The thermodynamic model adopted for the ORC system is based on a previously validated framework developed in our earlier works [17], and is here applied to evaluate the performance of a transcritical cycle under variable thermal input conditions. However, the evaporator model, which links the ORC system to the exhaust flow of the engine, has been specifically developed for this study and is described in detail in the following section.

The model assumes steady-state conditions for the quasi-static analysis at partial load and neglects pressure drops and heat losses. Thermophysical properties of the working fluids are retrieved from the REFPROP database. The net electric power output is calculated as:

$$P_{el} = \eta_{em,t} P_e - \frac{P_t}{\eta_{em,p}} \tag{9}$$

where P_e and P_p are the expander and pump powers, and $\eta_{em,t}$ and $\eta_{em,p}$ are the electromechanical efficiencies of the turbine and pump, respectively. The expander's isentropic efficiency was calculated via a generalized correlation proposed in a previous work [52]. It is derived from fitting experimental data available in scientific literature for various dynamic expanders. The correlation reflects the typical trend of increasing isentropic efficiency with expander size, as expressed in the following equation:

$$\eta_{is,e} = 53.94 P_{is,e}^{0.081} \tag{10}$$

where $P_{is,e}$ is the rated isentropic power of the expander, expressed in kilowatts. Furthermore, the thermal power input due to the engine waste gas is defined as:

$$\dot{Q}_{th} = \dot{m}_{exh}\left(T_{exh,in} - T_{exh,out}\right) \tag{11}$$

The ORC efficiency is then:

$$\eta_{ORC} = \frac{P_{el}}{\dot{Q}_{th}} \tag{12}$$

The effectiveness of low-temperature heat recovery heavily depends on the working fluid selection, which must be capable of efficiently extracting heat from the available source. The choice is driven by a combination of factors, including thermodynamic performance, environmental impact (e.g., GWP, ODP), safety (e.g., low flammability), and overall system design requirements.

For this study, a comparative analysis of three promising working fluids was conducted. Their main properties are summarized in Table 8. R245fa is already well established in the scientific literature, which could simplify its integration and adoption into existing vehicle architectures. Its proven performance and compatibility with current infrastructure make it a reliable choice. R1234ze(E) is a fourth-generation refrigerant from the hydrofluoroolefin (HFO) category, characterized by a very low environmental impact. Finally, isobutane (R600a) is distinguished by a high power-to-weight and power-to-volume ratio according to the literature [42]. Its favorable thermodynamic properties, i.e., critical pressure and temperature, density, and molar mass, allow for a more compact and lightweight system design, which is ideal for integration into space-constrained vehicles.

The saturation curves of the three fluids are depicted in Fig. 22. Table 9 shows the main parameters of the TORC under design conditions.

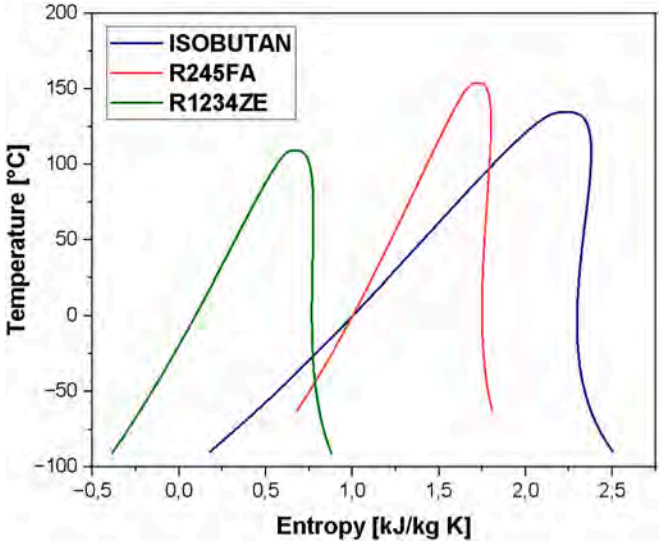

Fig. 22. Saturation curve of organic fluids used in the model.

Table 8
Specification of the organic fluids considered in this investigation.

Type fluid	Critical Temperature (°C)	Critical Pressure (kPa)	Critical (kg/m^3)	Molar Mass (kg/kmol)
R245fa	154	3650	516	134
R1234ze	109	3640	489	114
Isobutane	135	3630	225	58.1

The evaporator exploits the thermal power of the exhaust gases. Off-design performance of the turbine was evaluated using the Stodola ellipse approach. The pump operates with variable shaft speed to ensure the correct mass flow rate, while the condensation pressure and temperature are considered constant [27] and an iterative procedure is performed which ends when the physical feasibility of the solution is guaranteed [17]. The model has been validated in a previous work [17].

Table 9
Main input parameters to the ORC model.

Parameters	Unit	Values
Condensation Temperature	(°C)	30-40-50
Maximum temperature	(°C)	250
Maximum pressure	(-)	1.6 $p_{critical}$
Pump isentropic efficiency	(%)	70
Expander isentropic efficiency	(%)	Variable with size
Electro-mechanical efficiency	(%)	90
ICE outlet exhaust gas temperature	(°C)	350
Design outlet exhaust gas temperature	(°C)	90
Exhaust gas mass flow rate	(kg/s)	0.18

7.2.1. Heat exchange model and comparison

The heat exchanger is a key component in the ORC system, responsible for transferring thermal energy from the exhaust gases to the organic working fluid. This section presents the modeling approach adopted for the evaporator and compares two common configurations: plate heat exchangers (PHE) and shell-and-tube heat exchangers (STHE). Plate heat exchangers are characterized by a compact design and high thermal efficiency due to their large surface-to-volume ratio. However, they are typically limited to moderate pressure applications (usually up to 40 bar) and are less suitable when the pressure difference between the hot and cold sides is significant. They offer compactness and high heat transfer efficiency due to their large surface-to-volume ratio. However, they are generally limited to applications with moderate pressures (typically below 40 bar) and are less suitable for fluids with significantly different pressures on the hot and cold sides. In contrast, shell-and-tube heat exchangers are more robust and better suited for high-pressure applications, as they do not require gaskets and exhibit lower pressure drops—an important factor for WHR system efficiency. Shell-and-tube heat exchangers, on the other hand, offer greater mechanical robustness and are better suited for high-pressure conditions. Their gasket-free design and lower pressure drop make them preferable for WHR systems operating under demanding conditions.

The heat exchanger is discretized into 100 elementary sections, each characterized by a constant enthalpy difference [24]. For each section, the heat transfer rate is computed according to equation (1):

$$\dot{Q} = U_i A \Delta T_{log,i} = U_i A \frac{\Delta T_i - \Delta T_{i+1}}{ln\left(\frac{\Delta T_i}{\Delta T_{i+1}}\right)} \tag{13}$$

where U_i is the local overall heat transfer coefficient, A_i is the heat transfer area of the section, and $\Delta T_{log,i}$ is the logarithmic mean temperature difference between the exhaust gas and the working fluid at the inlet and outlet of the section.

In transcritical conditions, the convective heat transfer coefficient is estimated using the Jackson and Hall [53] correlation for the Nusselt number:

$$Nu_{of} = 0.0183 Re_{of}^{0.82} Pr^{0.5} \left(\frac{\rho_{wall}}{\rho_{of}}\right)^{0.3} \left(\frac{\bar{c}_p}{cp_{of}}\right)^{n} \tag{14}$$

where Re is the Reynolds number, Pr is the Prandtl number, ρ is the density, c_p is the specific heat capacity. The exponent n is equal to:

$$n = \begin{cases} 0.4, T_{of} < T_w < T_{pc} and T_{pc} < T_{of} < T_{wall} \\ 0.4 + 0.2\left(\frac{T_{wall}}{T_{pc}} - 1\right), T_{of} < T_{pc} < T_{wall} \\ 0.4 + 0.2\left(\frac{T_{wall}}{T_{pc}} - 1\right)\left[1 - 5\left(\frac{T_{of}}{T_{pc}} - 1\right)\right], T_{pc} < T_{of} < 1.2T_{pc} \end{cases} \tag{15}$$

The exponent n depends on the proximity to the pseudo-critical temperature The subscripts “of” and “wall” refer to the organic fluid and the wall, respectively. The pseudo-critical temperature is defined as the temperature at which the specific heat capacity of the organic fluid reaches a maximum at a pressure above the critical point. The wall temperature is approximated as the average between the temperatures of the organic fluid and the exhaust gas. The average specific heat of the working fluid is calculated as:

$$\bar{c}_p = \frac{h_{wall-}h_{of}}{T_{wall} - T_{of}} \tag{16}$$

where h_{wall} is the specific enthalpy of the fluid in contact with the wall

The convective heat transfer coefficient (h_{of}) of the organic fluid is calculated as

$$h_{of} = \frac{Nu_{of} k_{of}}{D_h} \tag{17}$$

Dove k_{of} e is the thermal conductivity and D_h is the hydraulic diameter (equal to the tube diameter in the STHE case). The overall heat transfer coefficient:

$$U = \frac{1}{\frac{1}{\alpha_{of}} + \frac{1}{\alpha_{exh}} + \frac{\delta}{k_{shell}} + R_f} \tag{18}$$

where h_{exh} is the convective coefficient of the exhaust gas, estimated using the Dittus-Boelter correlation, δ is the tube wall thickness and R_f is the fouling resistance. The total heat transfer area is computed as follows:

$$A_{tot} = \sum_{i=1}^{i=m} A_i = \frac{\dot{Q}_{exh,i,ICE}}{\Delta T_{log} * U} \tag{19}$$

where e $\dot{Q}_{exh,i,ICE}$ is the thermal power recovered by the Heat Exchanger in each section.

The main input parameters for the heat exchanger model are summarized in Table 9. The exhaust gas enters the evaporator at 350°C and exits at 90°C, with a mass flow rate of 0.18 kg/s. The maximum working fluid temperature is set to 250°C, and the maximum pressure is assumed to be 1.6 times the critical pressure of the selected organic fluid. These values are used as boundary conditions for the thermal sizing of the evaporator. The thermal effectiveness of the heat exchanger is defined as:

$$\varepsilon = \frac{\dot{Q}}{\dot{Q}_{max}} = \frac{\dot{m}_{org}(h_{org,out} - h_{org,in})}{\dot{m}_{exh} c_{pexh}(T^{in}_{exh} - T^{in}_{org})} \tag{20}$$

where $h_{org,out}$ and $h_{org,in}$ are the enthalpies of the working fluid at the evaporator outlet and inlet, respectively.

The same modeling approach was applied to simulate both PHE and STHE configurations. The two models differ in the definition of the hydraulic diameter and the heat transfer area. For the plate heat exchanger, the total heat transfer area is calculated as

$$A_{plate} = wLN^{\circ}_{plate} \tag{21}$$

where w and L are the plate width and length.

For the shell-and-tube heat exchanger, the area is computed as $A_{shelltube} = d_{external} * L * N^{\circ}_{tube} * \pi$, where $d_{external}$ is the external diameter of the tubes, L is the tube length, and N°_{tube} is the number of tubes.

7.2.2. Validation of the heat exchanger model

The heat exchanger model was validated using reference data from Karellas et al. [24], who investigated the design of plate heat exchangers for supercritical Organic Rankine Cycles (ORCs).

Table 10
Exchanger characteristics for validation [24].

Characteristics	Unit	Value		Reference value
Width	mm	100		
b (distance between plates)	mm	2		
δ (plate thickness)	mm	0.45		
Fluid	-	R134a		
n (number of section)	-	100	100	
Organic fluid Pressure	bar	50		50
Area	m^2	1.83		2.2
U (global heat exchange coefficient)	W/m^2K	2220		2500
ε (efficiency)	-	81%		83%
ΔT_{min}	°C	10.1		10

To validate the model, a simulation was performed replicating the geometric and operating conditions reported by Karellas et al. for R134a at 50 bar. The geometric configuration used in the simulation is summarized in Table 10.

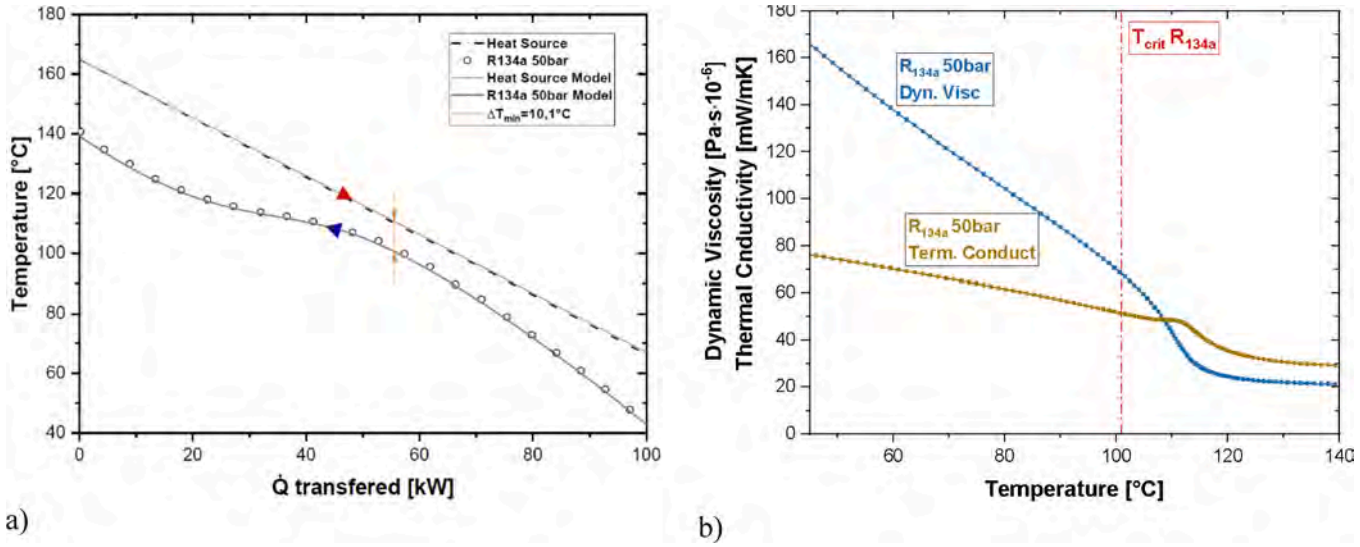

Fig. 23. validation plate heat exchanger model: a) T-Q diagram, b: dynamic viscosity and thermal conductivity [24].

The temperature profiles of the organic fluid and the exhaust gas, shown in Fig. 23(a), closely match the trends observed in Karellas et al., especially the characteristic inflection in the organic fluid curve caused by the peak in specific heat capacity near the pseudo-critical point. Fig. 23(b) shows the variation of dynamic viscosity and thermal conductivity with temperature and provides physical insight into the thermophysical mechanisms responsible for the shape of the curve of Fig. 23(a). These properties change rapidly near the pseudo-critical temperature, directly affecting the local heat transfer coefficient. This variation leads to a nonlinear heat transfer behavior, visible as a slope change in the organic fluid temperature curve. The strong sensitivity of heat transfer to these properties in the supercritical regime reinforces the importance of using temperature-dependent correlations in the model.

The simulated global heat transfer coefficient and thermal efficiency are in good agreement with the reference values, with relative errors of 2.80% and 2.17%, respectively. These results validate the accuracy of the model for the design and performance prediction of supercritical ORC heat exchangers.

Data availability

Data will be made available on request.

References

[1] Environment T&. Euro VII HD policy paper: Euro VI trucks still don't meet emission limits on the road 2021.
[2] Samaras ZC, others. A European Regulatory Perspective towards a Euro 7 Proposal 2022.
[3] Mohr D, Shipp T, Lu X. The Thermodynamic Design, Analysis and Test of Cummins' Supertruck 2 50% Brake Thermal Efficiency Engine System, Detroit, Michigan, United States: 2019, p. 2019-01–0247. Doi: 10.4271/2019-01-0247.
[4] Douadi O, Ravi R, Faqir M, Essadiqi E. A conceptual framework for waste heat recovery from compression ignition engines: Technologies, working fluids & heat exchangers. Energy Convers Manage: X 2022;16:100309. https://doi.org/10.1016/j.ecmx.2022.100309.
[5] Xu B, Rathod D, Yebi A, Filipi Z, Onori S, Hoffman M. A comprehensive review of organic rankine cycle waste heat recovery systems in heavy-duty diesel engine applications. Renew Sustain Energy Rev 2019;107:145–70. https://doi.org/10.1016/j.rser.2019.03.012.
[6] Peris B, Navarro-Esbrí J, Molés F, Martí JP, Mota-Babiloni A. Experimental characterization of an Organic Rankine Cycle (ORC) for micro-scale CHP applications. Appl Therm Eng 2015;79:1–8. https://doi.org/10.1016/j.applthermaleng.2015.01.020.
[7] Farhat O, Faraj J, Hachem F, Castelain C, Khaled M. A recent review on waste heat recovery methodologies and applications: Comprehensive review, critical analysis and potential recommendations. Cleaner Eng Technol 2022;6:100387. https://doi.org/10.1016/j.clet.2021.100387.
[8] Yang C, Li Y. Fuel-saving performance and main losses of an organic-Rankine-cycle-based exhaust heat recovery system in heavy truck application scenarios. Appl Therm Eng 2021;193:117025. https://doi.org/10.1016/j.applthermaleng.2021.117025.
[9] Broekaert S, Grigoratos T, Savvidis D, Fontaras G. Assessment of waste heat recovery for heavy-duty vehicles during on-road operation. Appl Therm Eng 2021;191:116891. https://doi.org/10.1016/j.applthermaleng.2021.116891.
[10] Mahmoudzadeh Andwari A, Pesiridis A, Karvountzis-Kontakiotis A, Esfahanian V. Hybrid electric vehicle performance with organic rankine cycle waste heat recovery system. Appl Sci 2017;7:437. https://doi.org/10.3390/app7050437.
[11] Thantla S, Aspfors J, Ghanbarpour M, Fridh J. Performance analysis of a dual-loop organic Rankine cycle system for waste heat recovery from engine coolant and exhaust of a heavy-duty truck. Appl Therm Eng 2023;219:119203. https://doi.org/10.1016/j.applthermaleng.2022.119203.
[12] Deshmukh PV. A comprehensive review of waste heat recovery from a diesel engine using organic rankine cycle. Energy Rep 2021;7:3951–70. https://doi.org/10.1016/j.egyr.2021.06.081.
[13] Li Z, Wang L, Jiang R, Wang B, Yu X, Huang R, et al. Experimental investigations on dynamic performance of organic Rankine cycle integrated with latent thermal energy storage under transient engine conditions. Energy 2022;246:123413. https://doi.org/10.1016/j.energy.2022.123413.
[14] Imran M, Haglind F, Lemort V, Meroni A. Optimization of organic rankine cycle power systems for waste heat recovery on heavy-duty vehicles considering the performance, cost, mass and volume of the system. Energy 2019;180:229–41. https://doi.org/10.1016/j.energy.2019.05.091.
[15] Villani M, Tribioli L. Comparison of different layouts for the integration of an organic Rankine cycle unit in electrified powertrains of heavy duty Diesel trucks. Energ Conver Manage 2019;187:248–61. https://doi.org/10.1016/j.enconman.2019.02.078.
[16] Lion S, Michos CN, Vlaskos I, Rouaud C, Taccani R. A review of waste heat recovery and Organic Rankine Cycles (ORC) in on-off highway vehicle Heavy Duty Diesel Engine applications. Renew Sustain Energy Rev 2017;79:691–708. https://doi.org/10.1016/j.rser.2017.05.082.
[17] Morrone P, Algieri A, Castiglione T. Hybridisation of biomass and concentrated solar power systems in transcritical organic Rankine cycles: a micro combined heat and power application. Energ Conver Manage 2019;180:757–68. https://doi.org/10.1016/j.enconman.2018.11.029.
[18] Pérez-Iribarren E, González-Pino I, Azkorra-Larrinaga Z, Gómez-Arriarán I. Optimal design and operation of thermal energy storage systems in micro-cogeneration plants. Appl Energy 2020;265:114769. https://doi.org/10.1016/j.apenergy.2020.114769.
[19] Sanaye S, Khakpaay N. Innovative combined optimization and modified maximum rectangle method for equipment sizing and operational strategy of an integrated system with cold thermal storage. Energy Rep 2022;8:137–60. https://doi.org/10.1016/j.egyr.2021.11.245.
[20] Joubert JW, Gräbe RJ. Real driving emissions data: Isuzu FTR850 AMT. Data Brief 2022;41:107975. https://doi.org/10.1016/j.dib.2022.107975.
[21] Al-mahmodi AF, Munusamy Y, Atta MR, Suyambulingam I, Bin Mokaizh AA, Muniyadi M. Utilizing phase change materials in thermal energy systems:

applications in waste heat recovery. Appl Therm Eng 2025;279:128003. https://doi.org/10.1016/j.applthermaleng.2025.128003.
[22] Manikandan S, Devarajan Y, Vickram S. Advancing thermal energy storage with industrial and agricultural waste-derived phase change materials: a path towards sustainable energy systems. Process Saf Environ Prot 2025;198:107068. https://doi.org/10.1016/j.psep.2025.107068.
[23] Lv Z, Guo J, Mao H, Dong Y. Experimental analysis of energy flow and carbon dioxide emissions in plug-in hybrid electric vehicles under different operation modes. Energ Conver Manage 2025;343:120223. https://doi.org/10.1016/j.enconman.2025.120223.
[24] Karellas S, Schuster A, Leontaritis A-D. Influence of supercritical ORC parameters on plate heat exchanger design. Appl Therm Eng 2012;33–34:70–6. https://doi.org/10.1016/j.applthermaleng.2011.09.013.
[25] Donateo T, Marti G, Mujahid T, Nuzzo F, Tundo S, Zezza L, et al. Preliminary design and assessment of a waste heat recovery system for a hybrid-electric heavy-duty vehicle. J Phys: Conf Ser (in Press) 2025.
[26] Song J, Li X, Wang K, Markides CN. Parametric optimisation of a combined supercritical CO2 (S-CO2) cycle and organic Rankine cycle (ORC) system for internal combustion engine (ICE) waste-heat recovery. Energ Conver Manage 2020;218:112999. https://doi.org/10.1016/j.enconman.2020.112999.
[27] Kim IS, Kim TS, Lee JJ. Off-design performance analysis of organic Rankine cycle using real operation data from a heat source plant. Energ Conver Manage 2017;133:284–91. https://doi.org/10.1016/j.enconman.2016.12.016.
[28] Villani M, Lombardi S, Tribioli L. Performance evaluation of a heavy-duty diesel truck retrofitted with waste heat recovery and hybrid electric systems. SAE Int J Elec Veh 2020;09:41–59. https://doi.org/10.4271/14-09-01-0004.
[29] Campana F, Bianchi M, Branchini L, De Pascale A, Peretto A, Baresi M, et al. ORC waste heat recovery in European energy intensive industries: energy and GHG savings. Energ Conver Manage 2013;76:244–52. https://doi.org/10.1016/j.enconman.2013.07.041.
[30] Di Battista D, Di Bartolomeo M, Villante C, Cipollone R. On the limiting factors of the waste heat recovery via ORC-based power units for on-the-road transportation sector. Energ Conver Manage 2018;155:68–77. https://doi.org/10.1016/j.enconman.2017.10.091.
[31] Fan P, Song G, Zhai Z, Wu Y, Yu L. Fuel consumption estimation in heavy-duty trucks: Integrating vehicle weight into deep-learning frameworks. Transp Res Part D: Transp Environ 2024;130:104157. https://doi.org/10.1016/j.trd.2024.104157.
[32] Baldasso E, Mondejar ME, Andreasen JG, Rønnenfelt KAT, Nielsen BØ, Haglind F. Design of organic Rankine cycle power systems for maritime applications accounting for engine backpressure effects. Appl Therm Eng 2020;178:115527. https://doi.org/10.1016/j.applthermaleng.2020.115527.
[33] Michos CN, Lion S, Vlaskos I, Taccani R. Analysis of the backpressure effect of an Organic Rankine Cycle (ORC) evaporator on the exhaust line of a turbocharged heavy duty diesel power generator for marine applications. Energ Conver Manage 2017;132:347–60. https://doi.org/10.1016/j.enconman.2016.11.025.
[34] Zhao M, Wei M, Tian G, Song P. Simulation of effects of ORC system installation on heavy-duty truck. Appl Therm Eng 2018;128:1322–30. https://doi.org/10.1016/j.applthermaleng.2017.09.114.
[35] Ma Z, Zhang K, Xiang H, Gu J, Yang M, Deng K. Experimental study on influence of high exhaust backpressure on diesel engine performance via energy and exergy analysis. Energy 2023;263:125788. https://doi.org/10.1016/j.energy.2022.125788.
[36] Di Bartolomeo M, Di Battista D, Fatigati F, Cau G, Cipollone R. Direct and Indirect Exhaust Heat Recovery from Turbocharged Heavy-Duty Engine, Capri, Italy: 2023, p. 2023-24–0122. Doi: 10.4271/2023-24-0122.
[37] Guzzella L, Sciarretta A. Vehicle Propulsion Systems: Introduction to Modeling and Optimization. Berlin, Heidelberg: Springer Berlin Heidelberg; 2013. doi: 10.1007/978-3-642-35913-2.
[38] Heywood JB. Internal combustion engine fundamentals. Second edition. New York: McGraw-Hill Education; 2018.
[39] Özener O, Yüksek L, Ergenç AT, Özkan M. Effects of soybean biodiesel on a DI diesel engine performance, emission and combustion characteristics. Fuel 2014;115:875–83. https://doi.org/10.1016/j.fuel.2012.10.081.
[40] Schuster A, Karellas S, Aumann R. Efficiency optimization potential in supercritical Organic Rankine Cycles. Energy 2010;35:1033–9. https://doi.org/10.1016/j.energy.2009.06.019.
[41] Pili R, Romagnoli A, Spliethoff H, Wieland C. Techno-economic analysis of waste heat recovery with ORC from fluctuating industrial sources. Energy Procedia 2017;129:503–10. https://doi.org/10.1016/j.egypro.2017.09.170.
[42] Pili R, Castro Pastrana JD, Romagnoli A, Spliethoff H, Wieland C. Working fluid selection and optimal power-to-weight ratio for ORC in Long-Haul trucks. Energy Procedia 2017;129:754–61. https://doi.org/10.1016/j.egypro.2017.09.116.
[43] Soldado JC, Pesyridis A, Sphicas P, Nikolakopoulos P, Markides CN, Deligant M. Axial turbo-expander design for organic rankine cycle waste-heat recovery with comparative heavy-duty diesel engine drive-cycle performance assessment. Front Mech Eng 2021;7:676566. https://doi.org/10.3389/fmech.2021.676566.
[44] Sun J, Peng B. Experimental study on steady-state operation of organic Rankine cycle system under different operating conditions. Sci Rep 2025;15:1041. https://doi.org/10.1038/s41598-024-84813-2.
[45] Srivastava M, Sarkar J, Sarkar A, Antony A. Fabrication and experimental investigation of a laboratory-scale organic Rankine cycle and data-driven optimization. Energy 2025;323:135905. https://doi.org/10.1016/j.energy.2025.135905.
[46] Feng X, Shi F, Qiao G, Li Y, Liu C. Integrating organic Rankine cycle with thermoelectric generator in various applications utilizing low-grade energy: a review. Sustainable Energy Technol Assess 2024;68:103882. https://doi.org/10.1016/j.seta.2024.103882.
[47] Royo P, Acevedo L, Ferreira VJ, García-Armingol T, López-Sabirón AM, Ferreira G. High-temperature PCM-based thermal energy storage for industrial furnaces installed in energy-intensive industries. Energy 2019;173:1030–40. https://doi.org/10.1016/j.energy.2019.02.118.
[48] Ahmad A, Anagnostopoulos A, Navarro ME, Maksum Y, Sharma S, Ding Y. A comprehensive material and experimental investigation of a packed bed latent heat storage system based on waste foundry sand. Energy 2024;294:130920. https://doi.org/10.1016/j.energy.2024.130920.
[49] Gomez JC. High-temperature phase change materials (PCM) candidates for thermal energy storage (TES). Applications 2011. https://doi.org/10.2172/1024524.
[50] Jiménez-Arreola M, Pili R, Dal Magro F, Wieland C, Rajoo S, Romagnoli A. Thermal power fluctuations in waste heat to power systems: an overview on the challenges and current solutions. Appl Therm Eng 2018;134:576–84. https://doi.org/10.1016/j.applthermaleng.2018.02.033.
[51] Donateo T, Mujahid T, Morrone P, Algieri A. Analysis and Simulation of Fuel Consumption and Emissions in a Heavy-Duty Diesel Truck under Real-World Driving Conditions for Hybridization and Waste Heat Recovery. SAE Technical Paper 2025. https://doi.org/10.4271/2025-24-0096. 2025–24-0096.
[52] Perrone D, Falbo L, Morrone P, Algieri A. Techno-economic investigation of integrated biodiesel internal combustion engines and transcritical organic Rankine cycles for small-scale combined heat and power generation. Energy Convers Manage: X 2023;20. https://doi.org/10.1016/j.ecmx.2023.100426.
[53] Hassani Mokarram N, Mosaffa AH. Investigation of the thermoeconomic improvement of integrating enhanced geothermal single flash with transcritical organic Rankine cycle. Energ Conver Manage 2020;213:112831. https://doi.org/10.1016/j.enconman.2020.112831.